Geol. Mag. **151** (*6*), *2014, pp. 1051–1071.* © *Cambridge University Press 2014*
doi:10.1017/S001675681300109X

Microstructural, compositional and petrophysical properties of mylonitic granodiorites from an extensional shear zone (Rhodope Core complex, Greece)

ROSALDA PUNTURO*†, ROSOLINO CIRRINCIONE*, EUGENIO FAZIO*, PATRIZIA FIANNACCA*, HARTMUT KERN‡, KURT MENGEL§, GAETANO ORTOLANO* & ANTONINO PEZZINO*

*Università degli Studi di Catania, Dipartimento di Scienze Biologiche, Geologiche e Ambientali, Corso Italia 57, I-95129 Catania (Italy)
‡CAU Universität, Institut für Geowissenschaften, Olshausenstr. 40, D-24098 Kiel (Germany)
§Technische Universität Clausthal, Institut für Endlagerforschung, Adolph-Roemer-Str. 2a, D-38678 Clausthal-Zellerfeld (Germany)

(*Received* 24 July 2013; *accepted* 10 December 2013; *first published online* 24 February 2014)

Abstract – At the southern boundary of the Rhodope Massif, NE Greece, the Kavala Shear Zone (KSZ) represents an example of the Eastern Mediterranean deep-seated extensional tectonic setting. During Miocene time, extensional deformation favoured syntectonic emplacement and subsequent exhumation of plutonic bodies. This paper deals with the strain-related changes in macroscopic, geochemical and microstructural properties of the lithotypes collected along the KSZ, comprising granitoids from the pluton, aplitic dykes and host rock gneisses. Moreover, we investigated the evolution of seismic anisotropy on a suite of granitoid mylonites as a result of progressive strain. Isotropic compressional and shear wave velocities (V_p, V_s) and densities calculated from modal proportions and single-crystal elastic properties at given pressure–temperature (*P–T*) conditions are compared to respective experimental data including the directional dependence (anisotropy) of wave velocities. Compared to the calculated isotropic velocities, which are similar for all of the investigated mylonites (average values: $V_p \sim 5.87$ km s^{-1}, $V_s \sim 3.4$ km s^{-1}, $V_p/V_s = 1.73$ and density $= 2.65$ g cm^{-3}), the seismic measurements give evidence for marked P-wave velocity anisotropy up to 6.92 % (at 400 MPa) in the most deformed rock due to marked microstructural changes with progressive strain, as highlighted by the alignment of mica, chlorite minerals and quartz ribbons. The highest P- and S-wave velocities are parallel to the foliation plane and lowest normal to the foliation plane. Importantly, V_p remains constant within the foliation with progressive strain, but decreases normal to foliation. The potential of the observed seismic anisotropy of the KSZ mylonites with respect to detectable seismic reflections is briefly discussed.

Keywords: mylonitic granitoid, petrofabric, seismic anisotropy, southern Rhodope Massif.

1. Introduction

Extensional mid-crustal shear zones are structural elements usually associated with the development of metamorphic core complexes (Davis & Coney, 1979; Lister, Banga & Feenstra, 1984; Wernicke, 1985; Dewey, 1988). These shear zones accommodate most of the strain and are considered to comply with the extensional tectonic process which accompanies and follows crustal thickening (Walcott and White, 1998; Pe-Piper, Piper & Matarangas, 2002; Gueydan, Mehl & Parra, 2005; Cirrincione *et al.* 2012). Another common feature of core complexes is the occurrence of granitoid plutons (Foster *et al.* 2001; Passchier, Zhang & Konopasek, 2005), many of which are considered to have syntectonically intruded during the active crustal-scale deformation stage.

Over the last decades, several studies have investigated the behaviour of high-strain zones as potential seismic reflectors, many of them focusing on the source of seismic anisotropy (e.g. Barruol *et al.* 1993; Rey, Fountain & Clement, 1994; Khazanehdari *et al.* 1998; Almqvist *et al.* 2013). In this view, the strong crystallographic orientations of constituent minerals and the mylonitic petrofabric play an important role in affecting the physical properties distribution along the shear zones (Fountain, Hurich & Smithson, 1984; Kern & Wenk, 1990; Burlini & Kunze, 2000).

The Kavala Shear Zone, exposed in the southern Rhodope (K. Kyriakopoulos, unpub. thesis, University of Athens, 1987) core complex (NE Greece, Fig. 1a), may be considered as a natural laboratory for investigating the mylonitic evolution of a magma intrusion, the emplacement and deformation of which took place during the shearing event. Well-preserved non-coaxial plastic deformation involved an early Miocene metaluminous to weakly peraluminous granodiorite pluton (named either Symvolon or Kavala in the literature) and metamorphic host rock, both locally intruded by aplitic dykes. Mylonitic rocks exhibit NE–SW

†Author for correspondence: punturo@unict.it

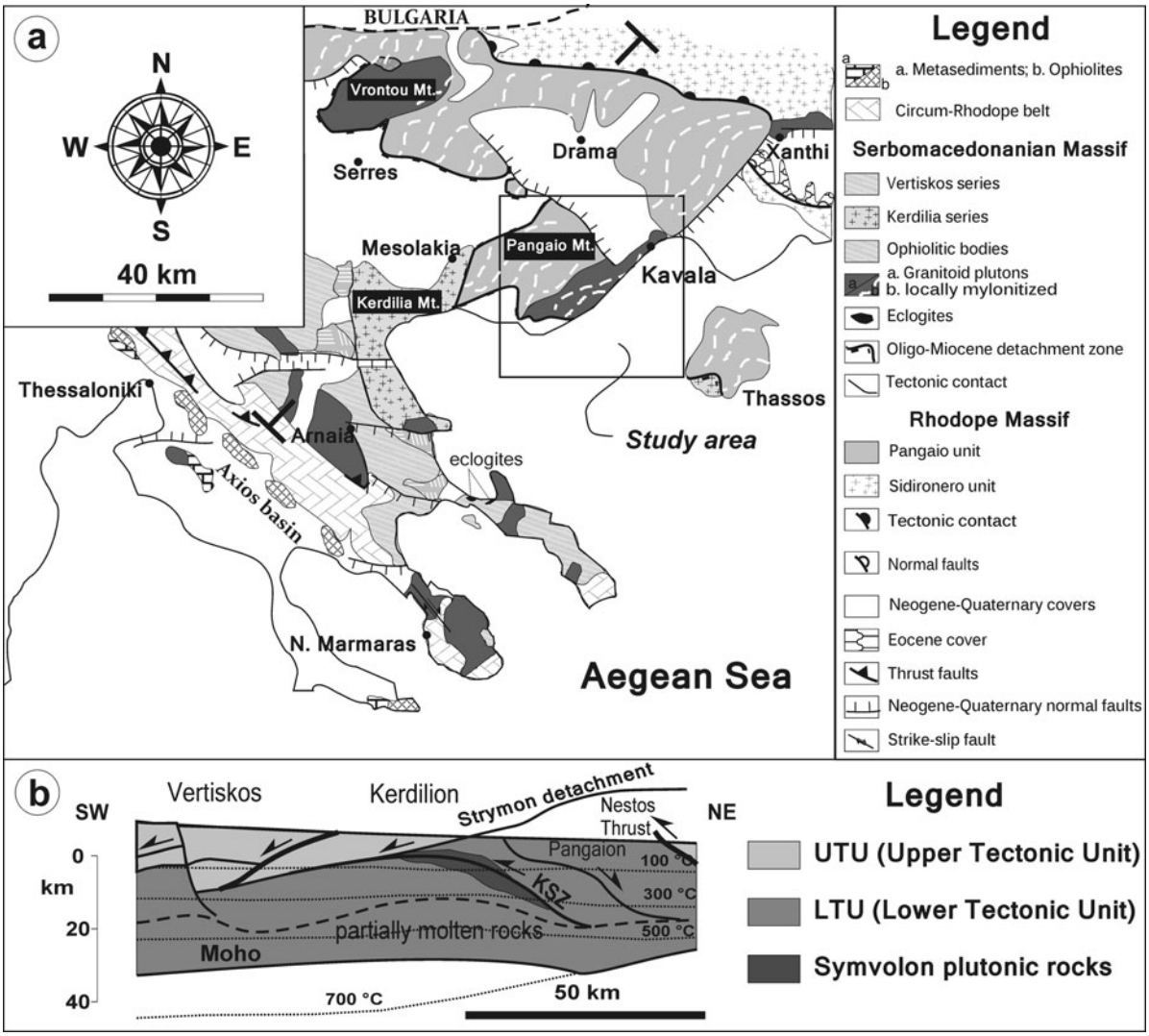

Figure 1. (a) Geological setting of the southern Rhodope and Serbo Macedonian massifs (modified after Brun & Sokoutis, 2007); and (b) synthetic cross-section of the area of interest.

monotonous stretching lineation consistent with the shape elongation of the exposed pluton, the deformation of which occurred at various stages during syn-shearing emplacement (Jones *et al.* 1992; Brun & Sokoutis, 2007).

The purpose of the present paper is to analyse and discuss the changes of composition and textural and petrophysical features in granitoid rocks sharing a mylonitic event during the evolution of an extensional shear zone; in particular, we attempted to highlight any local variation in seismic anisotropy related to increasing textural strength. Results obtained can promote a better understanding of the seismic behaviour of those present-day geodynamic realms characterized by exhumation after the crustal thickening stage.

2. Geological setting

The study area is located in NE Greece (Fig. 1a) in the southern part of the Rhodope Massif, mostly comprising pre-Alpine crystalline units intruded by various Cenozoic plutonic complexes. The Rhodope Massif is considered as a piece of the Alpine–Himalayan Orogen (Burg *et al.* 1996; Zagorchev, 1998; Kilias *et al.* 2010; Burg 2012), extended through southern Bulgaria and northern Greece, surrounded by the Balkan belt to the north and the Dinarides–Hellenides to the south (Dewey *et al.* 1973; Bonchev, 1988).

According to Dinter & Royden (1993) and Sokoutis *et al.* (1993) it can be considered as a 'Core Complex' exhumed by a large-scale extension that affected the north Aegean area during Eocene–Miocene time. It is bordered to the north by the Maritsa Fault, to the west by the Kerdilia Complex thrust units of the Serbo-Macedonian Massif in the Chalkidiki Peninsula (Kilias, Falalakis & Mountrakis, 1999) and to the east by early–middle Cenozoic volcanic sequences and sedimentary succession of the Thrace Basin (Jones *et al.* 1992; Caracciolo *et al.* 2012).

Papanikolaou & Panagopoulos (1981) subdivide the Rhodope Core Complex (RCC) into two main units: a Lower Tectonic Unit (LTU) and an Upper Tectonic Unit (UTU), corresponding to the Pangaio Unit and Sideronero Unit of Kilias & Mountrakis (1990),

https://doi.org/10.1017/S001675681300109X Published online by Cambridge University Press

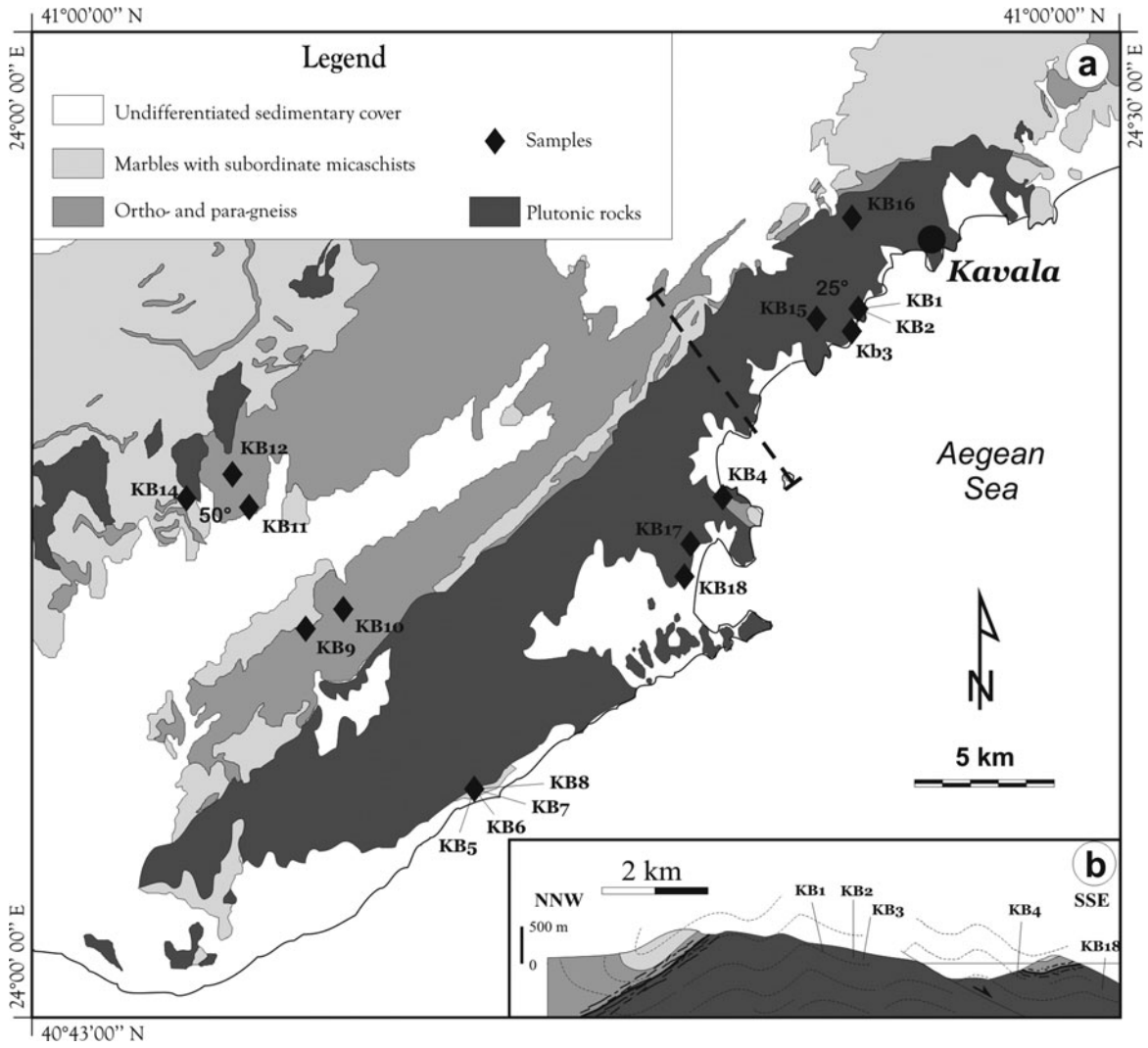

Figure 2. (a) Geological sketch map of the Kavala study area and samples location; and (b) profile (orientation: NNW–SSE) showing the anticline structure of the Kavala Shear Zone.

respectively (Fig. 1a, b). The two units are separated by a SW-verging thrust zone (Nestos thrust system of Lips, White & Wijbrans, 2000) extending from the Bulgarian border to the Xanthi Zone (Zachos & Dimadis, 1983; Kilias & Mountrakis, 1990). The LTU is mainly composed of massive and foliated marble rocks with subordinate paraschists in alternance with orthogneisses; the UTU consists of ortho- and paragneisses, sometimes migmatitic, amphibolites and ultramafic rocks, calc-silicate rocks and marbles (Fig. 2a). The orthogneiss protoliths are of Permo-Carboniferous age in the LTU and Late Jurassic age in the UTU, according to SHRIMP (sensitive high-resolution ion microprobe) U–Pb zircon dating by Turpaud & Reischmann (2010). These authors also proposed referring to the Lower and the Upper tectonic units as the Thracia Terrane and Rhodope Terrane, respectively.

The early–middle Cenozoic metamorphic evolution (see review by Burg, 2012) developed into three different events. The first event (M1), characterized by high-pressure conditions, produced eclogite facies assemblages within amphibolite and chloritoid-staurolite schists (Mposkos & Perdikatsis, 1987; Liati, 1988). The second event (M2) attained pressure–temperature (*P*–*T*) conditions of *c.* 0.7 GPa and 650 °C, overprinting the syn-M1 high-pressure assemblages. The last event (M3), showing retrograde character, developed under greenschist facies conditions. Geochronological data suggest an early–middle Eocene age for M2 (Liati, 1988), whereas the retrograde mylonitic event (M3?) affecting the basement gneisses in the Kavala area may be ascribed to early Miocene time (*c.* 19–22 Ma), indicating exhumation at shallow crustal levels (consistent with temperatures of 350–400 °C) by that time (Del Moro *et al.* 1990; Lips, White & Wijbrans, 2000).

As a consequence of the Eocene–Miocene large-scale extension, numerous sedimentary basins developed with associated effusive and intrusive magmatism (Jackson & White, 1989; Baker & Liati, 1991). The magmatic activity took place in close spatial association with the development of the extensional structures throughout NE Greece from the Chalkidiki Peninsula to eastern Thrace; indeed, these magmatic complexes represent the source area of the Thrace Basin sandstones (Caracciolo *et al.* 2011, 2013).

https://doi.org/10.1017/S001675681300109X Published online by Cambridge University Press

According to Jones *et al.* (1992) the various middle Cenozoic granitoids of the Rhodope Massif are mostly post-collisional crustal magmas, emplaced at the same time as extensional collapse of the over-thickened crust. They include: (1) the Xanthi granodiorite body (*c.* 30 Ma; K. Kyriakopoulos, unpub. thesis, University of Athens, 1987; Liati & Kreuzer, 1990) which crops out in the SE area close to the coastline; (2) the Vrondou granodiorite complex (*c.* 30 Ma; Durr *et al.* 1978; Kolocotroni & Dixon, 1991) which occupies the northern area of Serres town, evolving to mylonite in the western margin; and (3) the Kavala (or Symvolon) pluton (21–22 Ma; Dinter *et al.* 1995) cropping out in the SW sector of the Rhodope Massif, close to the city of Kavala (Fig. 2a). The Kavala pluton constitutes the core of an anticline (Fig. 2b); it is a NE–SW-elongated body *c.* 45 km long and 5–12 km wide and mainly consists of weakly to strongly foliated granodiorites (Kyriakopoulos, Pezzino & Del Moro, 1989; Neiva *et al.* 1996; Eleftheriadis & Koroneos, 2003). The Kavala and (the western part of the) Vroundou plutons are considered to be related to the same tectonic phase since they both show evidence of syn-extensional shearing emplacement (e.g. Gapais, 1989; Dinter & Royden, 1993; Dinter *et al.* 1995).

The Kavala (Symvolon) pluton investigated in this paper intruded pre-Miocene marbles and gneisses, including Permo-Carboniferous metagranitoids (Turpaud & Reischmann, 2010), of the LTU along the SW–NE-trending Kavala–Komotini fault zone (Dimadis & Zachos, 1989).

A crystallization pressure in the range of 0.53–0.75 GPa has been inferred by Neiva *et al.* (1996) using Al-in-hornblende geobarometry. Dinter *et al.* (1995) constrained intrusion, mylonitization and rapid cooling of the pluton to below 500 °C at *c.* 21–22 Ma (U–Pb zircon and titanite ages and Ar/Ar hornblende ages).

Syntectonic emplacement of the Kavala pluton is apparent from pervasive S-C-C′ fabric, with NE–SW-oriented stretching lineation and inferred top-to-the-SW or -WSW sense of shear (Brun & Sokoutis, 2007). Intensity of deformation increases towards the contact with the host rock gneisses that, according to the same authors, were already deformed during the emplacement of the pluton. Despite the longer deformation history of the host rock gneisses, possibly including the effects of Cretaceous thrusting, it is suggested that any previous linear fabric was affected by rotation towards the early Miocene principal stretching direction. All the fabric elements of the plutonic rocks as well as of the host rocks are therefore considered to reflect the latest horizontal stretching and to represent markers of the extensional shear zone activity (Punturo *et al.* 2012).

3. Method

Variably deformed lithotypes were collected along the shear zone, including granitoids from the pluton, aplite dykes and host rock gneisses (Fig. 2a, Table 1).

Table 1. Specimens collected and geographic coordinates.

Sample	Lithotype	North coordinate	East coordinate
KB1	Granodiorite	40° 55′ 07″	024° 22′ 52″
KB2	Granodiorite	40° 54′ 58″	024° 22′ 47″
KB3	Granodiorite	40° 54′ 48″	024° 22′ 38″
KB4	Granodiorite	40° 51′ 38″	024° 19′ 00″
KB5	Granodiorite	40° 46′ 42″	024° 12′ 15″
KB6	Aplite	40° 46′ 42″	024° 12′ 17″
KB7	Aplite	40° 46′ 42″	024° 12′ 17″
KB8	Granodiorite	40° 46′ 57″	024° 12′ 17″
KB9	Orthogneiss	40° 40′ 44″	024° 07′ 45″
KB10	Orthogneiss	40° 49′ 41″	024° 08′ 25″
KB11	Orthogneiss	40° 51′ 27″	024° 05′ 50″
KB12	Orthogneiss	40° 52′ 12″	024° 05′ 11″
KB14	Granodiorite	40° 51′ 56″	024° 04′ 32″
KB15	Granodiorite	40° 54′ 53″	024° 21′ 38″
KB16	Granodiorite	40° 56′ 40″	024° 22′ 33″
KB17	Granodiorite	40° 50′ 40″	024° 18′ 14″
KB18	Granodiorite	40° 50′ 40″	024° 18′ 14″

Petrographic investigations were carried out on thin-sections cut according to the fabric elements (i.e. *x*: stretching lineation; *y*: perpendicular to lineation within the foliation plane; and *z*: pole to foliation) assisted by X-ray fluorescence (XRF) bulk-rock chemistry analysis, electron probe micro-analysis of main and accessory mineral phases and calculation of modal abundances by means of PetMix spreadsheet (available at http://www.geologynet.com/micros2.htm).

This first step was aimed at highlighting the main petrographic and microstructural features of all of the analysed lithotypes involved in the shearing event. Subsequently, we focused on selected granitoid mylonites from the pluton since they were involved in a single deformational event and exhibit a relative compositional homogeneity, confirmed by both meso- and macroscale observations and by geochemical investigation.

Electron probe micro-analyses (EPMA) were performed with a Cameca SX100 at the Department of Geosciences, Mining and Economics, Clausthal University of Technology, equipped with a W-filament, four vertical wavelength-dispersive spectrometers, operating at 15 kV accelerating voltage and 20 nA beam current conditions, calibrated with natural mineral standards. Part of the analyses were also performed on a Tescan-Vega\\LMU scanning electron microscope (SEM), equipped with an energy-dispersive x-ray spectrometer (EDS) Edax Neptune XM4 60 at the Department of Biological, Geological and Environmental Sciences of Catania University.

Whole-rock compositions were determined by X-ray fluorescence on pressed powder pellets, performed on a Philips PW2404 spectrometer equipped with a Rh anticathode at the Department of Biological, Geological and Environmental Sciences, Catania University, corrected for matrix effects (Franzini, Leoni & Saitta, 1975). Loss on ignition (LOI) values were determined by standard gravimetric procedures. Diagrams displaying the geochemical variability of the studied rocks were constructed using the PetroGraph software by Petrelli *et al.* (2005).

https://doi.org/10.1017/S001675681300109X Published online by Cambridge University Press

The calculation of the mineral modes is based on the generalized petrological mixing model reported by Le Maitre (1979) using the computer program PetMix, which is based on least-squares fit.

Bulk elastic and density properties of the selected granitoid samples were first calculated at fixed P–T conditions on the basis of volume percentages of constituent minerals, their compositions and single crystal elastic moduli by considering the aggregate to be isotropic (Hacker & Abers, 2004).

Successively, seismic velocities (P- and S-wave) and density were experimentally measured at increasing pressure conditions (up to 400 MPa) in a multi-anvil apparatus using the ultrasound transmission technique (Kern 1982; Kern, Liu & Popp, 1997). The use of transducers operating at 2 MHz (V_p) and 1 MHz (V_s) allowed the measurement of the directional dependence (anisotropy) of elastic properties as a function of pressure.

Measurements of compressional and orthogonally polarized shear-wave velocities were made on 43 mm edged sample cubes cut parallel to macroscopic fabric elements (i.e. lineation, foliation). The shear-wave transducers were oriented such that the predominant S1 and S2 particle motions were either parallel or perpendicular to foliation and lineation. Each set of results is composed of nine velocity values: three P-wave velocities and six S-wave velocities. Length and volume (density) variations of the sample cubes, resulting from changes in the main stress, are obtained from the piston displacement. The cumulative error in both V_p and V_s was estimated to be <1 %. A detailed description of the device, as well as the transducer–piston–sample arrangement, is given by Kern, Liu & Popp (1997).

4. Outcrop features

The main rock type of the Kavala pluton is a medium- to coarse-grained, sometimes porphyritic, granodiorite composed of quartz, plagioclase and K-feldspar with varying proportions of biotite and hornblende as mafic phases. Hornblende-biotite diorites and tonalites, typically foliated, and monzogranites locally crop out. Dioritic-tonalitic enclaves are widespread and mostly concentrated at the pluton periphery. Aplitic dykes intrude the plutonic rocks as well as the metamorphic host rocks at different localities. At the scale of the outcrop (Fig. 3a–c) a pervasive S-C-C′ fabric, with NE–SW-oriented stretching lineation and inferred top-to-the-SW or -WSW sense of shear, is evident (Fig. 2a). The field-pervasive planar fabric, mostly consisting of C surfaces (strike 199°; dip 14° ESE), shows textures varying from weakly deformed to strongly mylonitic. In country rocks which were already deformed during the pluton emplacement, the mylonitic event lead to almost-complete obliteration of the original structural features (Fig. 3a, b). The intensity of shearing deformation in the plutonic rocks increases towards the contact with the country rocks, consistent with syn- to late-tectonic emplacement (Fig. 3a, b). This is also indicated by the occurrence of two different dyke populations: an older population consisting of sheared subconcordant dykes, parallelized soon after their emplacement to the mylonitic foliation of the host rocks (Fig. 3c), and a younger population of dykes cutting the same foliation at a high angle (see also Brun & Sokoutis, 2007).

All of the investigated mylonitic rocks of the two groups (i.e. granitoids and country rocks) exhibit the classical appearance of L-S (lineated and foliated) tectonites (Turner & Weiss, 1963) with a pronounced cataclastic overprint of varying degrees. The first group comprises mylonites derived from granodiorite (samples KB1–5, KB8, KB14–18) and from aplite dykes (samples KB6 and KB7); the second group includes four metamorphic host rocks (KB9–12).

5. Petrography

5.a. Mylonites from granitoid rocks and aplite dykes

Mylonites from the granitoid rocks are characterized by the assemblage Pl, Qtz, Kfs and Bt ± Am as fundamental phases and Aln, Ep, Ttn, Zrn, Ap, Fe-oxides, Wmca, Grt, Tur and Chl as the most common accessory phases (mineral abbreviations after Siivola & Schmid, 2007); representative mineral-chemical compositions are reported in Appendix A (see the online Supplementary Material available at http://journals.cambridge.org/geo). The rocks mostly consist of variously rounded feldspar porphyroclasts (submillimetre up to centimetre sized) wrapped by quartz levels alternating with discontinuous micaceous domains that define a typical augen-type structure (Fig. 4a–d). The main mylonitic foliation (C surface), corresponding to the field foliation, is often accompanied by the presence of variably angulated flattening surfaces (S) locally intersected by C′-type foliation due to the activation of synthetic fractures with respect to the sense of shear. Local strain localization led to the formation of millimetre-thick ultramylonitic layers characterized by cryptocrystalline matrix, locally visible in some specimens (Fig. 4c, d).

The largest porphyroclasts are almost exclusively composed of K-feldspar (up to 2 cm in size in the samples deformed at a lesser extent), locally characterized by euhedral plagioclase inclusions concentrically arranged with long axes parallel to the crystal-growth edges, as is typical of K-feldspar phenocrysts grown in magma (e.g. Vernon, 1986; Fig. 4b). Moreover, K-feldspar crystals are often fragmented into lenses parallel to the mylonitic foliation (forming bookshelf-sliding microstructures) and show undulose extinction. Myrmekites sometimes occur at the crystal rims (Fig. 4d).

Plagioclase (also producing augens up to 5 mm size) together with quartz comprise granoblastic levels alternating with micaceous levels. Primary albite twins are also widespread; magmatic oscillatory zoning is sometimes evident (Fig. 4f).

The mineral chemistry of feldspars is relatively homogeneous in all of the examined plutonic rocks with

https://doi.org/10.1017/S001675681300109X Published online by Cambridge University Press

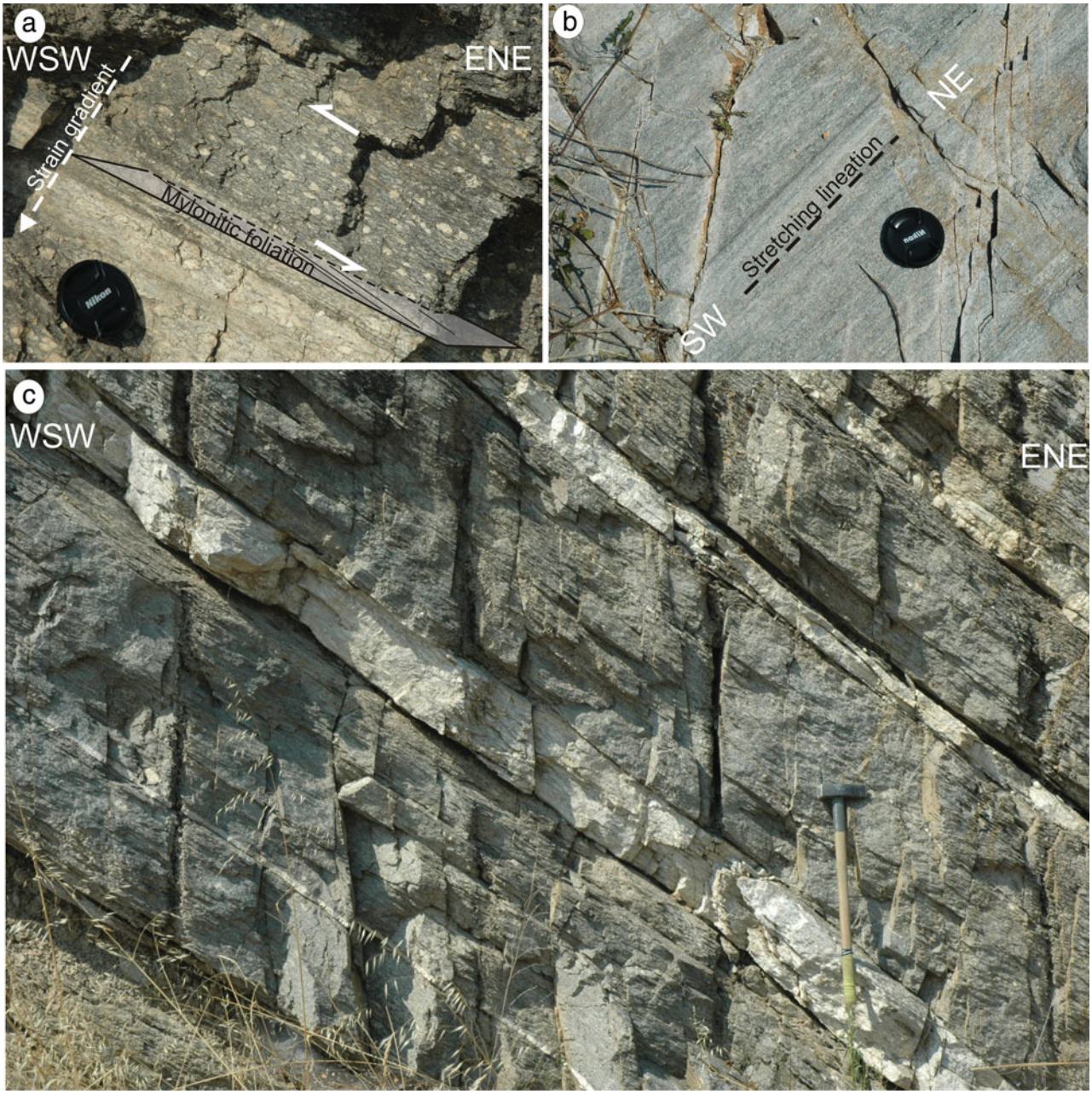

Figure 3. (Colour online) Mylonitic structures of country rocks: (a) evidence of mylonitic foliation and increasing strain within orthogneiss and (b) stretching lineation within orthogneiss. (c) Mylonitized granodiorite and aplite dykes.

alkali feldspar characterized by a nearly pure orthoclase composition and plagioclase ranging from andesine/oligoclase to albite (Fig. 5a); this latter composition is ascribed to synmylonitic retrograde reaction.

Quartz grains usually exhibit deformation lamellae, undulose extinction and sometimes chessboard patterns (Fig. 4g). Ribbon-like quartz is widespread, especially in the most-deformed samples; moreover, various recrystallization processes have been detected in quartz-rich domains such as bulging, subgrain rotation and grain boundary migration.

Biotite is the main mafic phase together with amphibole when it occurs in the assemblage. As is expected in mylonites, the biotite laths show characteristic sigmoidal shape forming 'mica-fish' (Fig. 4e). Fe/Fe + Mg ratios range from 0.36 to 0.52, with a slight Al^{IV} increment in biotite from amphibole-free granodiorite (Fig. 5a).

Amphibole often forms sigmoidal grains (Fig. 4h), delineating the S-C-C′ fabric together with Pl and Kfs. According to the classification diagrams depicted in Figure 5, relatively homogeneous edenite to pargasite compositions cluster at the boundary between the Fe-edenite, edenite-hornblende and Fe-pargasite-hornblende fields.

White mica and chlorite occur as products of synmylonitic reactions (Cirrincione *et al.* 2010). White mica is characterized by low phengite content and low Fe/Fe + Mg ratios; chlorite shows ripidolitic to pycnochloritic composition.

https://doi.org/10.1017/S001675681300109X Published online by Cambridge University Press

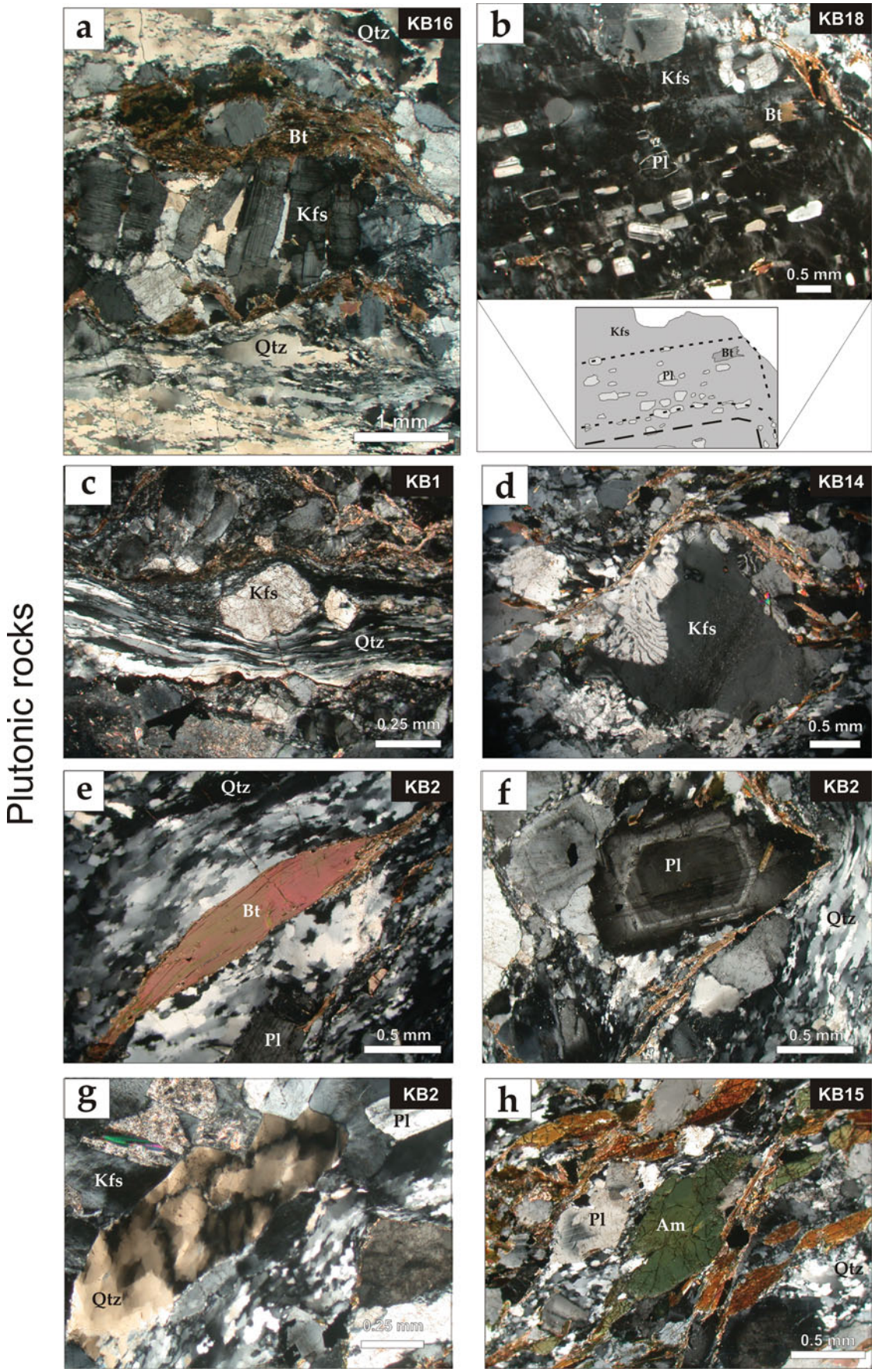

Figure 4. (Colour online) Photomicrographs (crossed polarizers) of selected mylonitic granodiorite: (a) alternance of quartz and micaceous domains that mantle feldspar porphyroclasts; (b) concentric distribution of plagioclase inclusions within K-feldspar megacryst; (c) quartz ribbons and microcrystalline matrix wrapping K-feldspar porphyroclast; (d) myrmekite developed at the periphery of a K-feldspar porphyroclast; (e) biotite fish mantled by recrystallized quartz grains; (f) relic magmatic zoning in plagioclase; (g) chessboard pattern within a quartz domain; and (h) sigmoidal plagioclase and amphibole porphyroclasts.

https://doi.org/10.1017/S001675681300109X Published online by Cambridge University Press

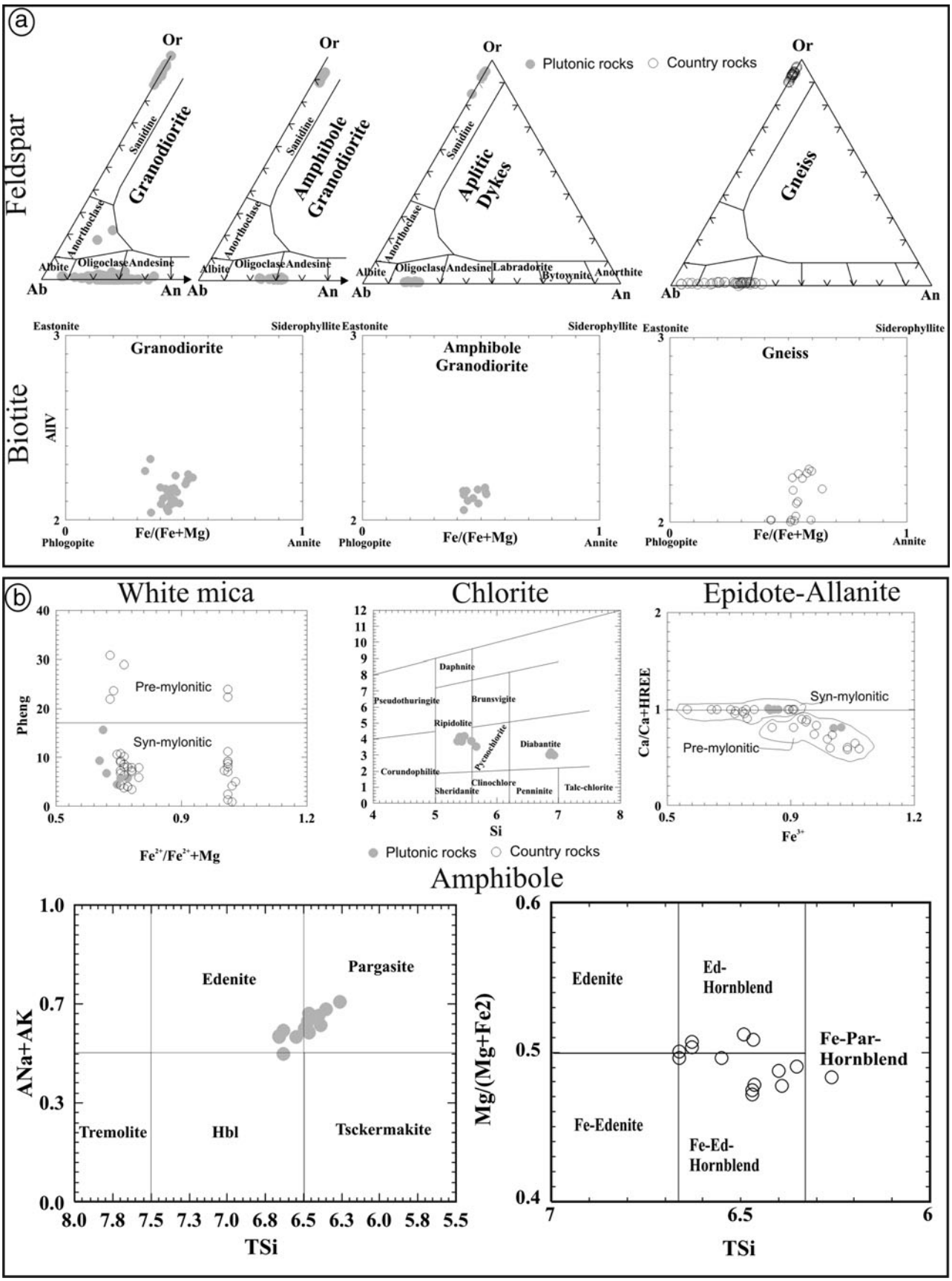

Figure 5. Compositional features of (a) fundamental and (b) accessory mineral phases of mylonitic rocks from the Kavala Shear Zone.

https://doi.org/10.1017/S001675681300109X Published online by Cambridge University Press

Among the accessory phases, allanite is widespread; it occurs as small grains which may be either pre- and syn-kinematic. Finally, very rare garnet fragments form swarms parallel to the main foliation.

From granitoid mylonitic rocks, we further selected a suite of specimens which we considered to be representative of the development of strain; indeed, these samples are characterized by progressively decreasing grain size, which accompanies diminishing porphyroclasts percentage (from 53.9 to 17.6 %) and increasing matrix content (from 46.2 to 82.4 %) as similarly observed in rocks from other shear zones (e.g. Cirrincione *et al.* 2009, 2010; Fazio, Punturo & Cirrincione, 2010).

The aplite dykes exhibit a fine grain size and are characterized by the assemblage Qtz, Pl, Kfs, Ep, Grt, Ap, Wmca, Ttn, Aln, Chl and Fe-oxides ± Bt.

Feldspar grains are usually cloudy due to very abundant crypto-crystalline inclusions of secondary phases and form fragmented and boudinaged porphyroclasts draped by quartz ribbons (Fig. 5a, b). Finer grain sizes, scanty biotite and relatively homogeneous plagioclase (oligoclase), together with the diabantite composition of synmylonitic chlorite, are the main differences from granodiorites (Fig. 5).

5.b. Country rocks

The second group of sampled mylonitic rocks comprises four orthogneisses (KB9–12) with the general assemblage Qtz, Pl, Kfs, Wmca and Bt, the latter mostly retrogressed into chlorite. Ap, Ep, Aln, Zrn, Ttn, Fe-oxides, Tur and Grt are the accessory constituents occurring at variable extent. Ultramylonite bands as well as S-C-C′ fabric are also visible (Fig. 6c, d); quartz domains are characterized by well-developed ribbon-like microstructure (up to 3 cm in length). White mica commonly occurs in these S-C-C′ mylonites, forming the classical 'fish' microstructure (Wmca1) characterized by a relatively high phengite content ranging from 17 to 30 % and variable Fe/Fe + Mg ratios (Fig. 5b). Moreover, fine-grained aggregates developed along the shear planes (Wmca2, Fig. 6g). Biotite is relatively abundant and characterized by an intermediate Fe/Fe + Mg ratio (Fig. 5a).

Synkinematic epidote coronas commonly surround pre-mylonitic allanite grains (Fig. 6e, f). The bending of feldspar twins often records an intense deformational event (Fig. 6h). Atoll-like garnet (very small grains, maximum 90 microns) surrounded by biotite laths may also occur.

6. Geochemistry

Samples from both granitoids and country rock orthogneisses involved in the Kavala Shear Zone have been analysed for major and selected trace elements; results are reported in Table 2.

In the Q′(F′)-ANOR classification diagram (Streckeisen & Le Maitre, 1979; Fig. 7a) the Miocene plutonic rocks and host gneisses mostly plot as two distinct groups in the granodiorite and in the granite fields, respectively. Aplite dykes show granite composition. The granodiorites are subalkaline and mostly metaluminous to weakly peraluminous (Fig. 7b), with ASI (aluminium saturation index) in the 0.99–1.06 range, except for an amphibole-bearing and relatively SiO_2-poor sample (KB15) with a lower ASI value of 0.91. For the other samples, no clear correlation between peraluminosity and SiO_2 content is observable. It is worth noting that both dykes and country rock gneisses show a more pronounced peraluminosity than main granodiorite types.

Compared to the compositions and trends reported by Neiva *et al.* (1996) and Eleftheriadis & Koroneos (2003) for the same Miocene granitoid rocks, no significant difference is observed. In the variation diagrams for major and selected trace elements (Fig. 8), despite diffuse data scattering granodiorites and aplite dykes follow the same magmatic trends of decreasing MgO, Fe_2O_{3tot}, TiO_2, Al_2O_3, P_2O_5, V and Zr and increasing K_2O and Rb with increasing SiO_2 content. Negative correlations are also envisaged for CaO, Na_2O, Sr and La. Country-rock othogneisses are often similarly scattered but they plot as a distinct population, defining trends subparallel to those of granodiorites, characterized by higher Fe_2O_{3tot}, TiO_2 and V and lower CaO, Na_2O and Sr for a given SiO_2 content. Since many major and trace elements appear to have been only slightly disturbed by post-magmatic modifications, their trends can be considered largely representative of the igneous protoliths of the different lithotypes, helping to select the most-suitable samples for the purposes of the present study.

Whole-rock chemical data together with mineral chemistry results were also used to calculate the modal composition of the studied rocks, based on the generalized petrological mixing model reported by Le Maitre (1979) using the spreadsheet PetMix. Results (Table 3; Fig. 9) provided the average percentages for plutonic granodiorite as follows: Qtz 29.2 – Pl 44.5 – Kfs 16 – Bt 8.1 being three samples characterized by the occurrence of hornblende 0.9, 2.5 and 15 vol. % in samples KB18, KB17 and KB15, respectively. The latter sample also exhibits the lowest quartz amount (23.9 %). Regarding the aplite dykes (samples KB7 and KB6), their modal percentages are: Qtz 32.4 and 36.2 vol. %; Pl 39.2 and 30.8 vol. %; and K-fsp 25.7 and 28.1 vol. %. Biotite occurs only in sample KB6 (4.9 vol. %), whereas in sample KB7 it is completely replaced by chlorite (2.7 vol. %).

Meta-igneous country rocks exhibit the following contents of main minerals: quartz 25.7–37.9 vol. %; plagioclase 28.4–49.5 vol. %; K-feldspar 9.4–23.5 vol. %; biotite 4.2–12.4 vol. % and white mica 4.7–18.5 vol. %, the latter absent from sample KB11.

7. Petrophysical properties

Petrophysical investigation focused on samples KB1, KB2, KB3, KB4 and KB18, which are considered to be representative of the increasing strain within the

https://doi.org/10.1017/S001675681300109X Published online by Cambridge University Press

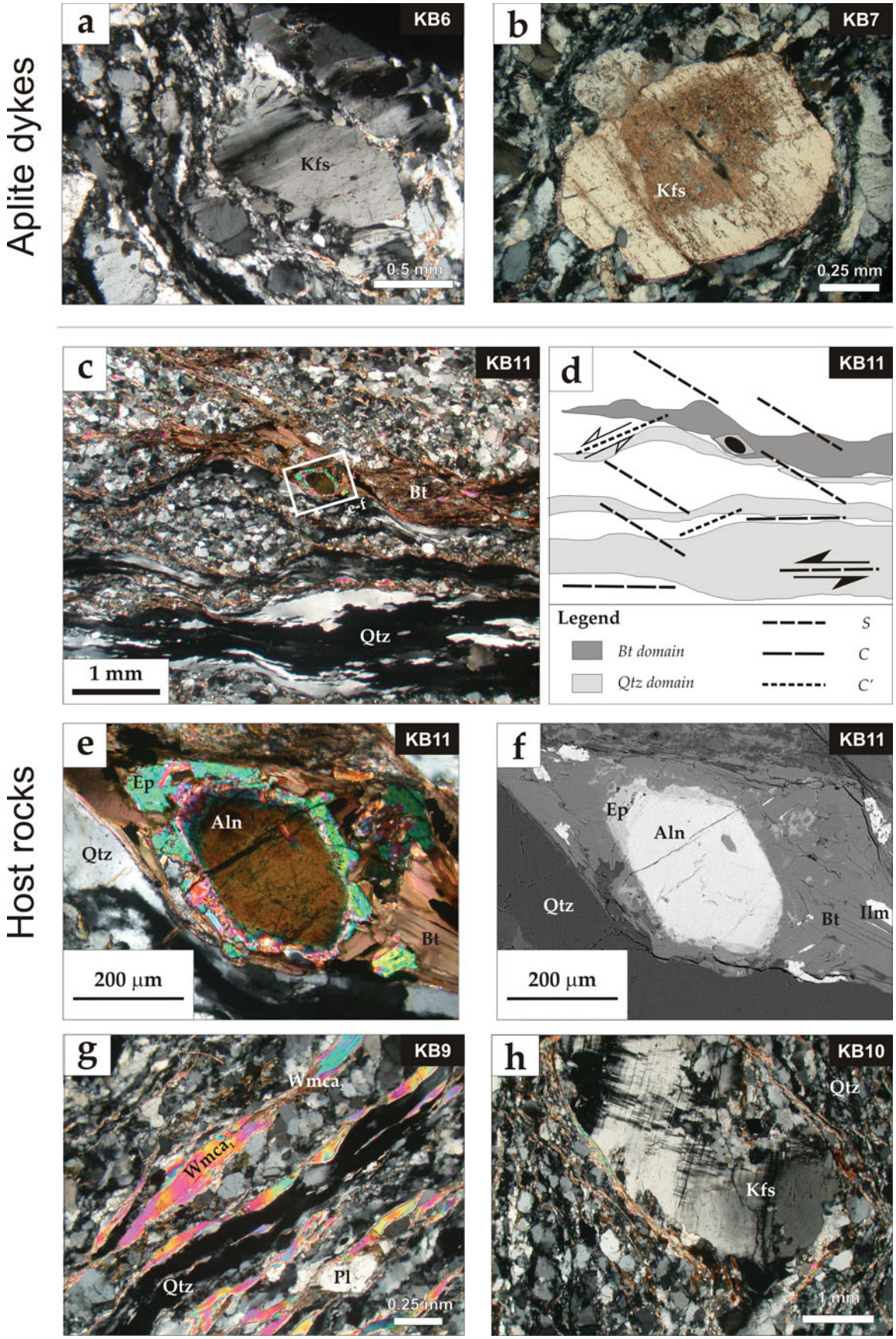

Figure 6. (Colour online) Photomicrographs of (a, b) aplite dykes and (c–h) host rocks. (a, b) K-feldspar porphyroclasts surrounded by quartz-mica formed matrix; (c, d) alternance of micaceous and quartz layers, development of S-C-C′ foliations and sinistral shearing sense; (e, f) close-up of rectangular area highlighted in (c): epidote corona surrounding pre-kinematic allanite (optical microscope) and SEM image; (g) alternance of micas and quartz domains along the shear planes; and (h) banding within feldspar.

https://doi.org/10.1017/S001675681300109X Published online by Cambridge University Press

Table 2. Whole rock (wt%) and selected trace element (ppm) compositions of mylonitic rocks from the Kavala Shear Zone. LOI – loss on ignition; b.d. – below limits of detection.

	Miocene plutonic rocks											Miocene dykes		Pre-Miocene orthogneisses			
Rock type Sample	KB1	KB2	KB3	KB4	KB5	KB8	KB14	KB15	KB16	KB17	KB18	KB6	KB7	KB9	KB10	KB11	KB12
SiO_2	71.28	71.45	71.15	69.10	68.53	69.27	69.98	65.11	69.38	70.96	71.49	75.24	74.34	72.88	74.12	70.58	72.92
TiO_2	0.19	0.18	0.19	0.29	0.17	0.26	0.23	0.47	0.25	0.21	0.21	0.05	0.07	0.23	0.16	0.39	0.19
Al_2O_3	15.27	15.40	15.15	15.96	17.03	15.80	15.87	15.12	15.96	15.40	15.33	14.08	14.56	15.24	13.95	14.90	14.57
Fe_2O_{3tot}	1.69	1.69	1.74	2.53	1.76	2.29	2.02	5.29	2.32	1.75	1.92	0.53	0.83	1.84	1.60	3.23	1.81
MnO	0.09	0.08	0.11	0.06	0.05	0.05	0.08	0.22	0.05	0.06	0.05	0.00	0.01	0.02	0.04	0.06	0.03
MgO	0.58	0.53	0.65	0.95	0.65	0.75	0.69	2.49	1.04	0.69	0.58	0.09	0.15	0.46	0.40	0.82	0.44
CaO	2.74	2.20	2.77	2.98	2.90	3.02	2.42	4.14	2.78	2.64	2.49	0.94	0.99	0.55	0.78	2.59	1.11
Na_2O	4.08	3.95	3.89	4.00	4.50	4.00	4.25	4.15	4.17	3.70	3.86	3.45	4.42	3.33	3.19	3.30	2.91
K_2O	3.39	3.69	3.62	3.13	3.07	3.03	3.87	2.07	3.31	3.95	3.50	4.94	3.94	3.89	4.68	3.33	4.82
P_2O_5	0.09	0.08	0.09	0.14	0.08	0.12	0.12	0.16	0.12	0.09	0.08	0.01	0.02	0.13	0.04	0.11	0.03
LOI	0.61	0.76	0.64	0.85	1.27	1.41	0.49	0.77	0.63	0.54	0.49	0.67	0.67	1.42	1.06	0.69	1.16
Sr	456	408	449	610	837	433	1146	427	517	330	359	270	326	128	62	147	59
V	10	10	13	23	14	16	12	48	21	12	14	3	3	b.d.	9	26	11
Cr	2	3	2	4	5	2	4	12	6	8	4	2	1	3	3	5	2
Co	7	8	7	10	7	7	8	19	10	8	7	1	4	8	7	12	9
Ni	2	2	3	3	4	3	4	8	4	7	5	b.d.	3	b.d.	1	3	2
Zn	31	30	34	98	19	21	31	45	11	22	24	7	7	24	26	47	28
Rb	144	157	180	115	88	83	110	129	106	120	115	163	107	139	171	134	210
Y	20	15	17	15	13	5	17	26	20	11	12	6	15	13	20	24	28
Zr	134	119	134	151	170	122	168	134	126	102	116	45	80	103	79	141	81
Nb	10	9	13	8	4	2	8	14	8	4	3	3	5	9	5	7	8
Ba	690	659	747	790	1013	698	1540	317	627	528	617	282	711	541	302	499	230
La	24	24	21	18	33	29	50	18	26	21	18	7	6	23	16	25	21
Ce	45	31	42	34	69	51	97	30	49	41	21	6	6	45	36	61	33
Pb	40	40	52	39	42	32	89	31	23	26	30	65	69	30	31	15	29
Th	18	15	16	16	24	13	43	13	16	18	14	6	7	15	23	19	21

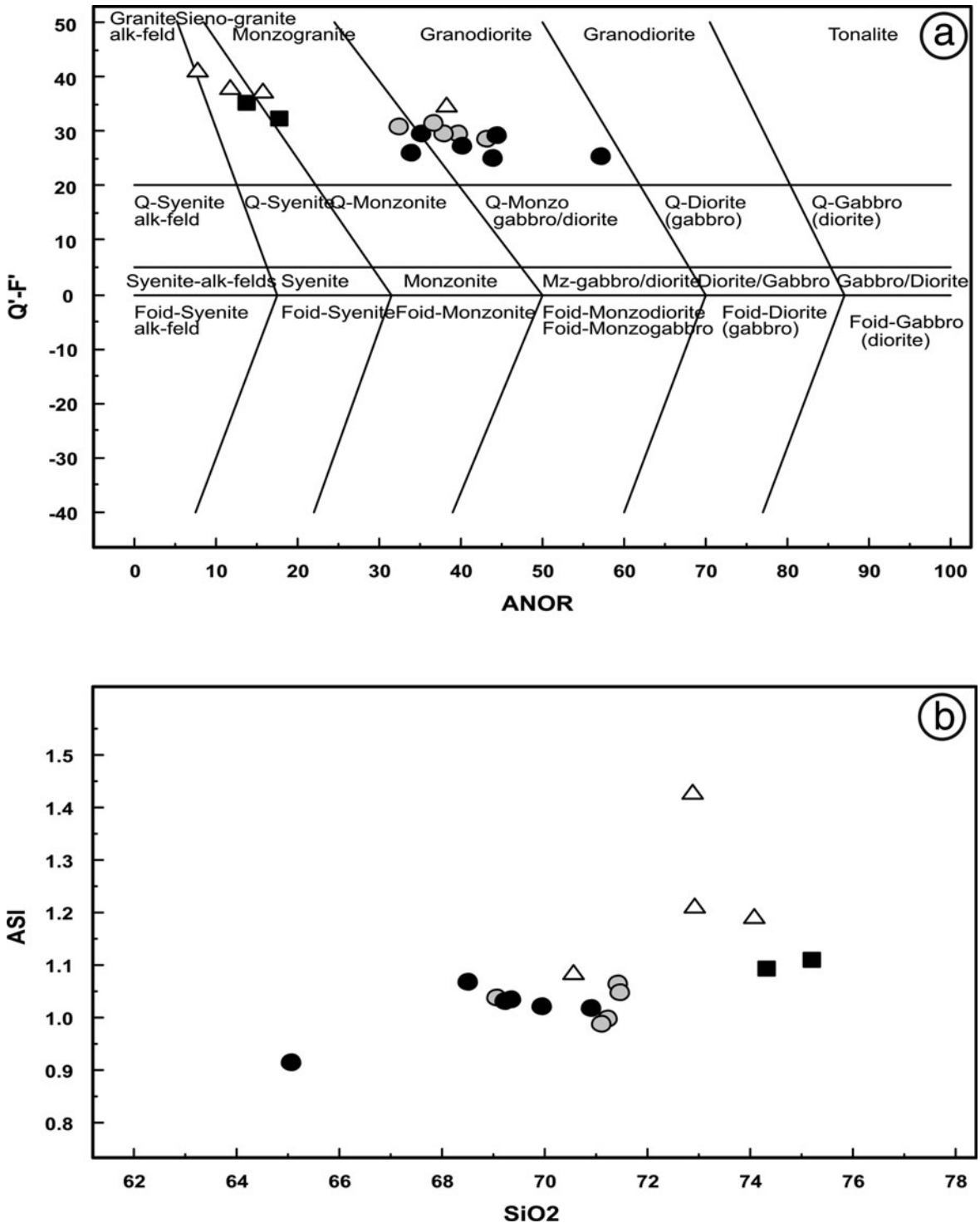

Figure 7. (a) Classification of the studied rocks from the Kavala Shear Zone in the Q′(F′)-ANOR diagram (Streckeisen & Le Maitre, 1979); (b) ASI v. SiO_2 variation diagram. Circles: Miocene plutonic rocks (the empty circles are the samples selected for the petrophysical investigation); squares: Miocene aplite dykes; triangles: pre-Miocene host rocks.

shear zone (Fig. 10); moreover, the selected samples are characterized by bulk and mineral compositions, which suggests a similar pre-mylonitic protolith (Figs 7–9).

The physical properties of these granitoid mylonites were first calculated by considering the aggregate to be isotropic, on the basis of the modal assemblage (calculated using PetMix) and of the single crystal elastic moduli; the computation of bulk modulus, shear modulus and density was carried out using the worksheet by Hacker & Abers (2004) based on thermodynamic relationships and on the Hashin–Shtrikman approximation. The calculated compressional and shear wave velocities for given P–T conditions are listed in Table 4. Since the investigated mylonites are homogeneous in compositions, results are very similar with $V_p \sim 5.87$ km s^{-1} and $V_s \sim 3.40$ km s^{-1}. Poisson's ratio is 0.25 for all of the investigated samples and, similarly, $V_p/V_s = 1.73$.

https://doi.org/10.1017/S001675681300109X Published online by Cambridge University Press

Table 3. Modal abundances (vol. %) of constituent minerals calculated using PetMix spreadsheet on the basis of bulk rock and mineral compositions.

Vol. %	Quartz	Plagioclase	K-feldspar	Biotite	White mica	Chlorite	Epidote	Hornblende
KB1	30.7	45.3	16.4	7.5	0.0	0.0	0.0	0.0
KB2	29.7	43.7	19.4	7.3	0.0	0.0	0.0	0.0
KB3	30.5	43.7	17.8	8.0	0.0	0.0	0.0	0.0
KB4	29.8	45.3	13.2	10.2	0.0	0.0	1.4	0.0
KB5	25.7	49.5	16.1	7.9	0.0	0.0	0.8	0.0
KB6	36.2	30.8	28.1	4.9	0.0	0.0	0.0	0.0
KB7	32.4	39.2	25.7	0.0	0.0	2.7	0.0	0.0
KB8	30.5	45.7	13.2	9.7	0.0	0.0	0.9	0.0
KB9	37.9	30.1	9.4	4.2	18.5	0.0	0.0	0.0
KB10	35.6	30.5	23.5	5.7	4.7	0.0	0.0	0.0
KB11	34.9	39.9	12.9	12.4	0.0	0.0	0.0	0.0
KB12	36.1	28.4	23.0	6.0	6.5	0.0	0.0	0.0
KB14	27.9	44.5	19.3	8.2	0.0	0.0	0.0	0.0
KB15	23.9	46.1	7.0	8.0	0.0	0.0	0.0	15.0
KB16	27.6	48.4	14.2	9.8	0.0	0.0	0.0	0.0
KB17	30.5	39.9	21.9	5.2	0.0	0.0	0.0	2.5
KB18	31.2	42.6	18.0	7.3	0.0	0.0	0.0	0.9

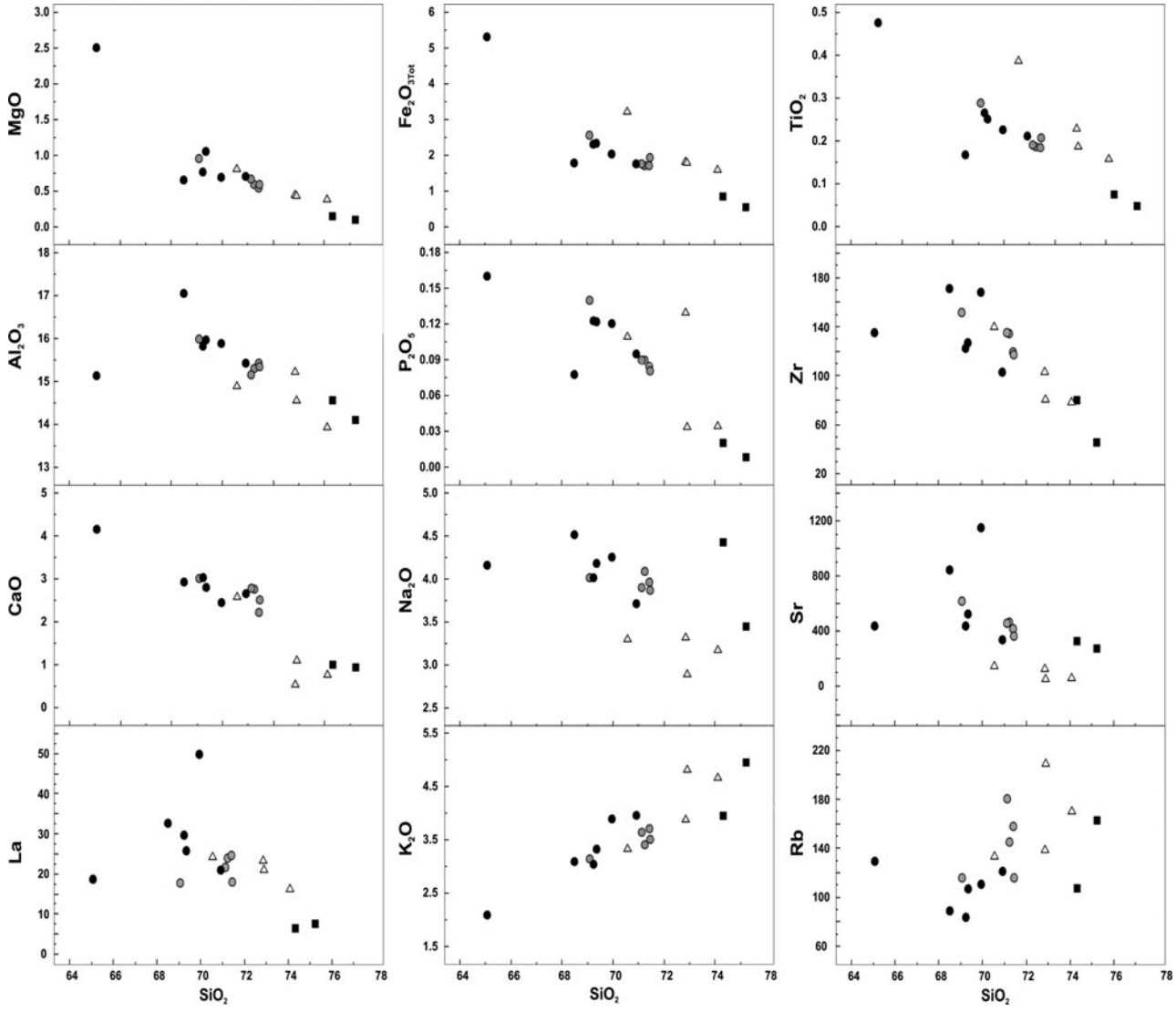

Figure 8. Harker variation diagrams for selected major and trace elements. Oxide amounts in wt %; trace elements in ppm. Symbols as in Figure 7.

https://doi.org/10.1017/S001675681300109X Published online by Cambridge University Press

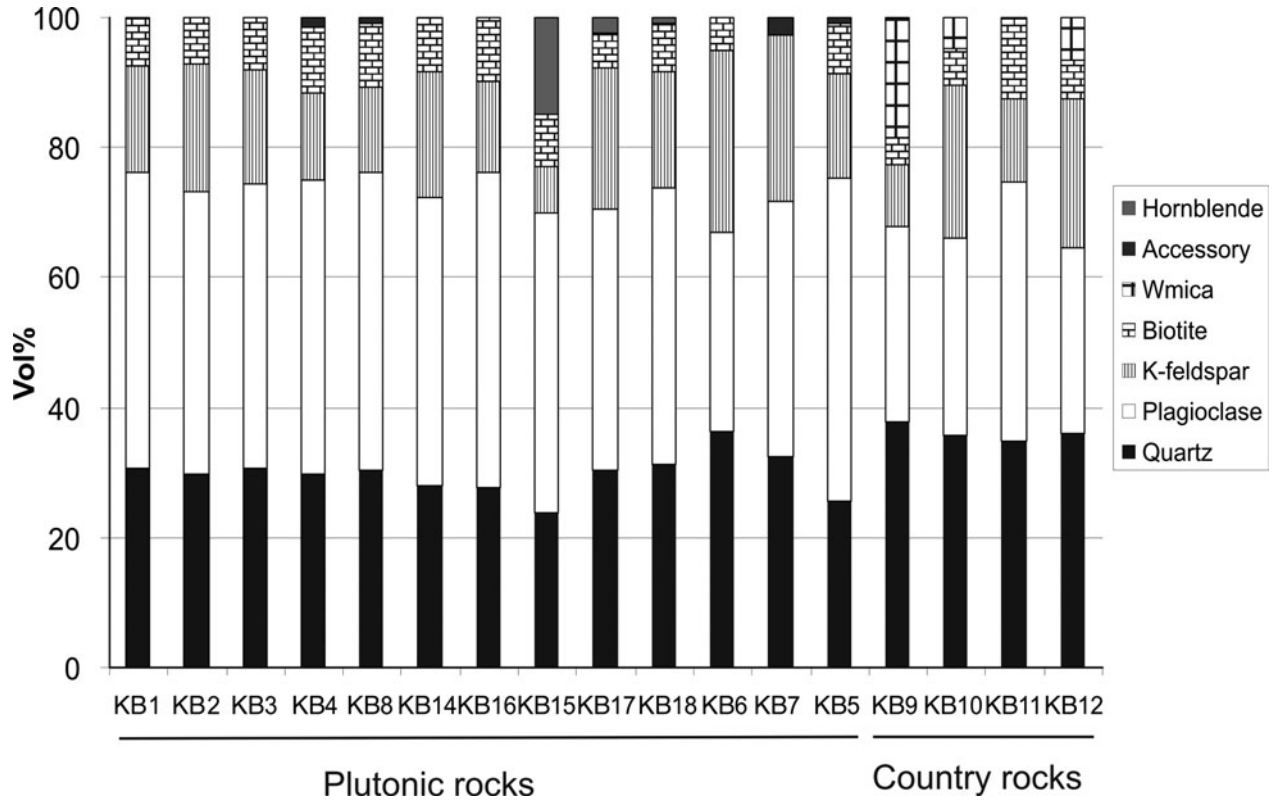

Figure 9. Modal abundances of the mylonitic rocks investigated, calculated on the basis of bulk rock and mineral chemistry.

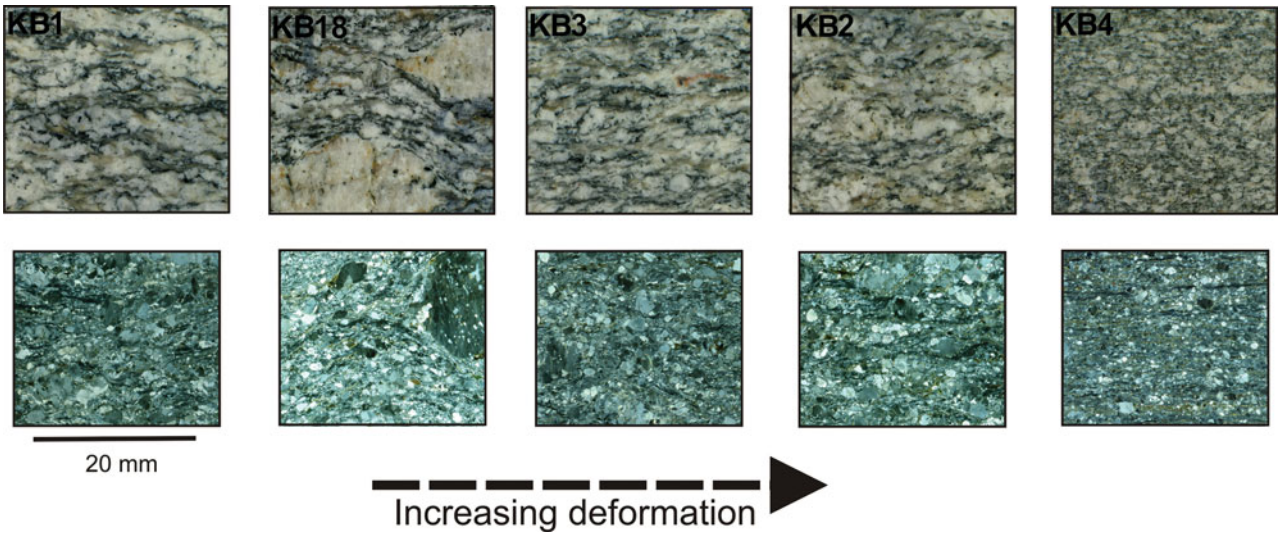

Figure 10. (Colour online) Photographs of the granodiorite mylonitic rock selected for the petrophysical investigation, illustrating the variation in microstructural features at both hand and micro scale.

In order to determine the directional dependence of seismic velocities on the same mylonitic rocks, measurements were carried out as a function of pressure (P_{max} = 400 MPa) on sample cubes cut according to the fabric elements (*x*: lineation; *x*–*y*: foliation plane; *z*: pole to foliation). Results for compressional and shear waves are listed in Appendix B (see the online Supplementary Material available at http://journals.cambridge.org/geo).

The pressure dependence of compressional wave velocities is shown in Figure 11, which summarizes the P-wave behaviour along the three mutually orthogonal directions together with the related anisotropy, defined as $[(V_{max}-V_{min})/V_{mean}]\times 100$. A non-linear rise of velocities is observed at low confining pressure, due to the progressive closure of oriented low-aspect-ratio microcracks that give rise to a steep decrease in seismic anisotropy.

At high-pressure conditions the compacted aggregates reflect a nearly intrisic behaviour, that is, the properties of the rock matrix. The intrinsic properties are controlled by the contribution of the constituent minerals, their abundances and arrangement in the rock. For all the studied mylonites, the highest P-wave

https://doi.org/10.1017/S001675681300109X Published online by Cambridge University Press

Table 4. Comparison between the physical properties calculated with the Hashin-Shtriman approximation (Hacker & Abers, 2004) and near-intrinsic properties measured at 400 MPa.

Calculated physical properties	KB1	KB2	KB3	KB4	KB18
Density (g cm^{-3})	2.63	2.63	2.63	2.65	2.63
V_p (km s^{-1})	5.87	5.87	5.86	5.87	5.88
V_s (km s^{-1})	3.40	3.39	3.39	3.39	3.39
Poisson ratio	0.25	0.25	0.25	0.25	0.25
V_p/V_s	1.73	1.73	1.73	1.73	1.72
Bulk modulus K (GPa)	50.03	50.28	50.04	50.61	50.22
Shear modulus G (GPa)	30.32	30.21	30.25	30.37	30.63
Measured physical properties (400 MPa)					
Density (g cm^{-3})	2.67	2.64	2.66	2.65	2.66
V_p (km s^{-1})	5.96	5.85	5.93	5.75	5.84
V_s (km s^{-1})	3.52	3.44	3.48	3.39	3.49
Poisson ratio	0.23	0.24	0.24	0.23	0.22
V_p/V_s	1.69	1.70	1.70	1.70	1.67

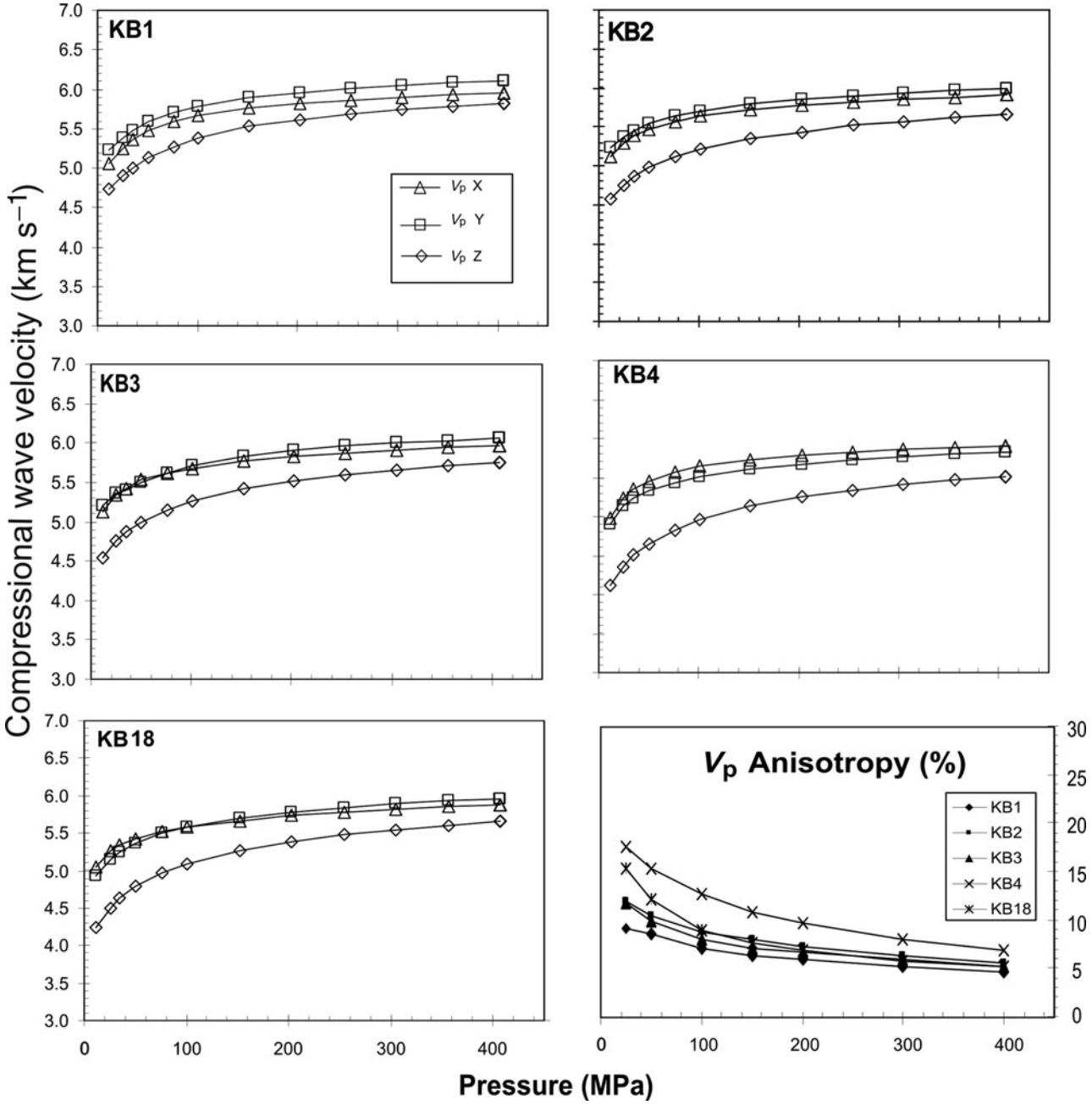

Figure 11. Patterns of compressional wave velocities (km s^{-1}) and related seismic anisotropy AV_p (%) as a function of pressure for the selected mylonitic granodiorite rocks (x: lineation; y: normal to lineation within the foliation plane; z: normal to foliation).

https://doi.org/10.1017/S001675681300109X Published online by Cambridge University Press

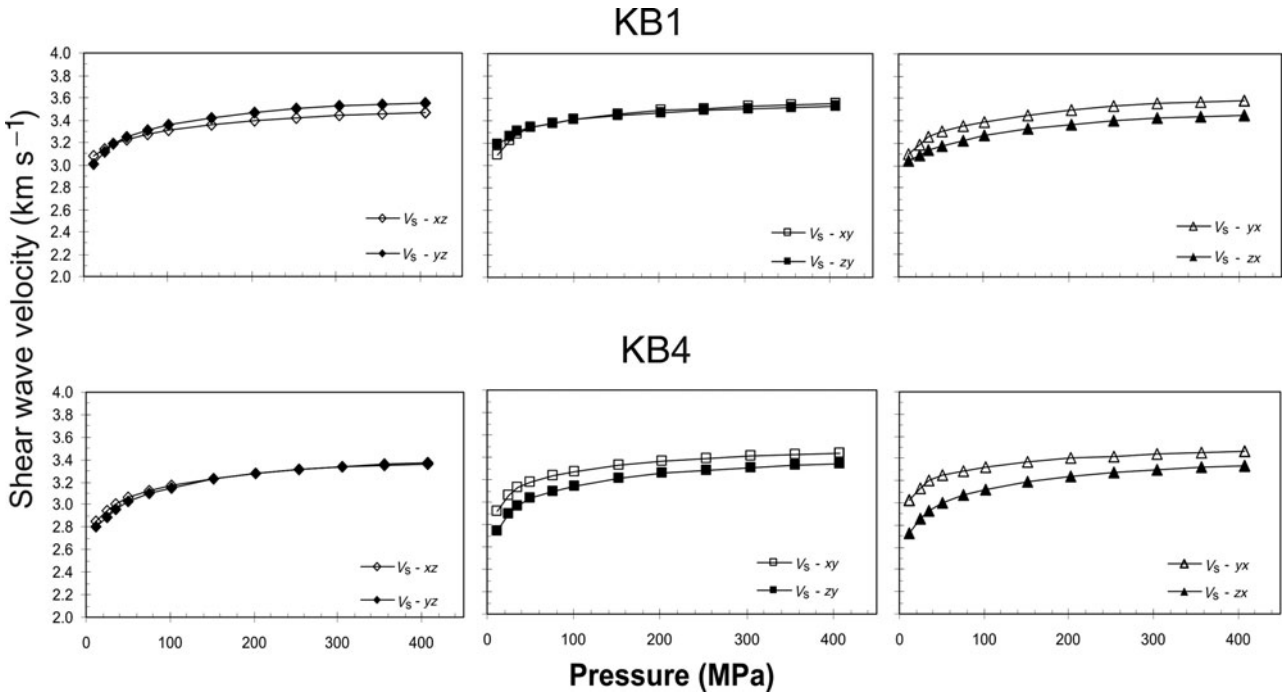

Figure 12. Patterns of shear wave velocities (km s^{-1}) for KB1 (weakly deformed) and KB4 (the most deformed) mylonitic granodiorite. The fabric elements (x, y and z) are as for Figure 11.

velocities are measured parallel to the foliation (x–y) plane whereas P-wave velocities are lowest normal to foliation (z-direction) (Fig. 11). At 400 MPa, compressional wave velocities of granodiorites lie within a narrow range ($V_{p,mean}$ = 5.75–5.96 km s^{-1}) as well as density (*c.* 2.66 g cm^{-3}). Seismic anisotropy of V_p increases from 4.66 % (sample KB1) to 6.92 % (sample KB4), with a V_p/V_s ratio of 1.70.

The shear waves velocities of the different rocks vary within the range 2.91–3.52 km s^{-1}. They depend on the propagation direction as well as on the direction of their polarization: fast and slow shear waves are polarized parallel and normal to the foliation plane, respectively. Shear wave splitting (S1–S2) is most pronounced within the foliation plane (Appendix B; see the online Supplementary Material available at http://journals.cambridge.org/geo) whereas, normal to foliation, the shear wave splitting is found to be low. Figure 12 depicts the detailed behaviour of shear waves with increasing pressure in samples KB1 and KB4, representative end-members of low- and high-strain domains within the granitoid mylonites. Finally, a comparison between measured and calculated results shows that velocities (both compressional and shear waves) as well as density values are very close (Table 4).

We also performed a regression analysis of the velocity–pressure relationship for both the non-linear and linear segments of the curves obtained at increasing pressure conditions. Interpolation was carried out using the VpPlot script (Wang *et al.* 2005) on MatLab. This tool provides information about critical points, velocity–pressure curve fitting and error analysis. In the non-linear regime, $V(P) = a(\ln P)^2 + b(\ln P) + c$ ($P = P_c$), where a and b are constants and c is the velocity when P is equal to 1 MPa. In the linear regime, the velocity–pressure relationship is described by $V(P) = V_0 + DP$ ($P < P_c$), where P_c is the critical confining pressure above which a linear velocity increase is observed. In the studied mylonite granodiorites, the linear behaviour is approached for $P_c > 250$ MPa. Intrinsic pressure derivatives of velocities, P_0, V_0 and P_c are listed in Tables 5 (compressional waves) and 6 (shear waves and V_p/V_s ratio).

It is worth noting that the petrophysical properties derived from the linear regime reflect the intrinsic behaviour of the rock, where the contribution of pores and microfractures is negligible.

For the studied mylonitic rocks, the relationship between microstructural features related to increasing strain (expressed as clast/matrix percentage) and elastic properties (represented by the anisotropy of V_p) is summarized in Figure 13.

Finally, we calculated the normal incidence reflection coefficients (R_c) from modelled and measured V_p and density values for the contacts between orthogneiss (sample KB10, representative of the country rock) and the mylonitic granodiorite (KB4 and KB1, the most- and least-deformed samples respectively; Table 7). When considering the rocks to be isotropic (both orthogneiss and granodiorite), reflection coefficients of *c.* 0.01–0.02 resulted. In order to envisage any possible reflector within the shear zone, we calculated the coefficients for all of the investigated mylonite granodiorite (KB1, KB2, KB3, KB4 and KB18) by considering, for each sample, the velocity distribution in the x–y (foliation) plane and in the z-direction (normal to foliation). Results highlight that the reflection coefficient remains similar (R_c = 0.02) in the samples

https://doi.org/10.1017/S001675681300109X Published online by Cambridge University Press

Table 5. Parameters for compressional wave velocity – pressure relationship and derivatives (calculated with VpPlot).

				$V_p = V_0 + DP$			$V_p = a(\ln P)^2 + b(\ln P) + c$			
Sample	P_c (MPa)	V_c (km s^{-1})	P_0 (MPa)	V_0 (km s^{-1})	$D = dV_p/dP$ (10^{-4} km s^{-1} MPa^{-1})	R^2	a (km s^{-1} MPa^{-2})	b (km s^{-1} MPa^{-1})	c (km s^{-1})	R^2
KB1	272	5.715	134	5.475	8.810	0.990	− 0.0041	0.3820	3.702	0.996
KB2	261	5.531	124	5.275	9.810	0.998	0.0083	0.2559	3.850	0.998
KB3	253	5.602	124	5.334	10.576	0.997	0.0039	0.3339	3.634	0.997
KB4	286	5.389	132	5.073	11.058	0.997	− 0.0082	0.4978	2.837	0.998
KB18	270	5.516	132	5.208	11.394	0.996	0.0003	0.4272	3.117	0.998

Table 6. Parameters for shear velocity – pressure relationship and derivatives (calculated with MatLab Program VpPlot), together with Poisson and V_p/V_s ratios.

	$V_s = V_0 + DP$				
Sample	V_{s0} (km s^{-1})	$D = dV_p/dP$ (10^{-4} km s^{-1} MPa^{-1})	R^2	Poisson (400 MPa)	V_p/V_s (400 MPa)
KB1	3.41	2.874	0.990	0.23	1.69
KB2	3.33	2.886	0.991	0.24	1.70
KB3	3.32	4.150	0.946	0.24	1.70
KB4	3.25	3.375	0.993	0.23	1.70
KB18	3.31	4.772	0.970	0.22	1.67

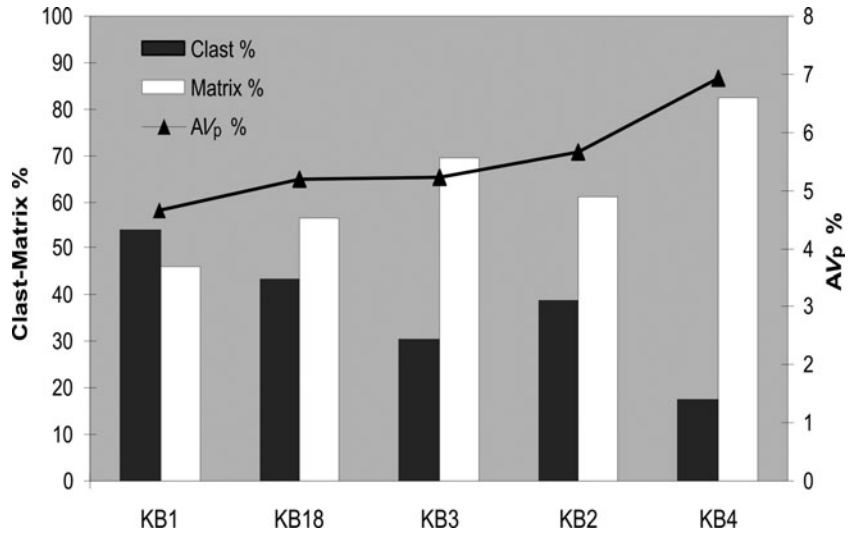

Figure 13. Clast (matrix) abundances in the selected mylonitic granodiorite together with AV_p (%) plot.

Table 7. Calculation of acoustic impedance I and normal incidence reflection coefficients R_c for the main lithotype of the Kavala Shear Zone.

Lithotype	I (10^6 kg m^{-2} s^{-1})	R_c
Average orthogneiss	15.58	0.01
Average mylonitc granodiorite	15.90	
KB1 (low anisotropy granodiorite)		
Foliation	16.10	0.02
Normal to foliation	15.55	0.02
KB4 (high anisotropy granodiorite)		
Foliation	15.54	0.03
Normal to foliation	14.60	

deformed at a lesser extent, whereas it increases to 0.03 in sample KB4 (the most-deformed mylonite; Table 7).

8. Discussion and concluding remarks

The extensional shear zone of Kavala is an excellent natural site for studying the relationship between mylonitic features and seismic properties in a syntectonic granodiorite pluton emplaced during the large-scale extension that affected NE Greece during late Cenozoic time.

Focusing on the main rock type of the pluton (i.e. granodiorite), we selected a suite with textural and compositional features representative of progressive deformation of the same granitoid rock across the shear zone (Fig. 10). Indeed, this assumption (based on mineralogical and geochemical features of the

https://doi.org/10.1017/S001675681300109X Published online by Cambridge University Press

selected samples) is justified by their similar elastic properties, calculated for the isotropic aggregates (Table 4).

Within the selected mylonite suite, the clast/matrix ratios dramatically decrease (from 1.2 to 0.2) as deformation proceeds. At the same time, quartz ribbons become widespread and micas tend to align parallel to mylonitic foliation. An addition, synmylonitic microstructures and new assemblages tend to replace the pre-mylonitic magmatic structures. In terms of changes in elastic properties and their distribution related to the rock fabric, we noted that within the shear zone the maxima in V_p, V_s and V_{s1} are within the foliation (x–y) plane, whereas the minima in V_p, V_s and V_{s2} tend to align normal to the mylonitic foliation. In particular, despite the fact that the compressional wave velocities remain quite constant within the foliation plane (*c.* 6 km s^{-1}), we observed a progressive velocity decrease normal to foliaton (z-direction) as deformation proceeds (Fig. 11). As a consequence, V_p anisotropy increases from 4.66 % (in areas deformed at a lesser extent) to 6.92 % in the most mylonitized domains (Fig. 13). Bulk anisotropy of the rocks is mainly caused by the phyllosilicate minerals (micas, chlorite), their modal abundances and crystal preferred orientation (CPO); indeed, as deformation proceeds and the angle between the S and C planes (S-C-C′ fabric) becomes smaller, the [001] axes tend to align parallel to the pole of the shearing plane. On the contrary, feldspars (which represent the load-bearing framework phases) probably make a negligible contribution to seismic anisotropy because of their brittle behaviour which does not produce appreciable CPO (Fig. 3a–h).

These results are also in agreement with recent studies on magnetic fabric, which highlighted a prevailing NE–SW-trending magnetic lineation and subhorizontal foliation planes (Zananiri *et al.* 2013) within the KSZ, confirming the high anisotropy character of the granitoid pluton which underwent ductile shearing of variable extent.

Importantly, the calculated normal incidence reflection coefficients (R_c) between the mylonitic granodiorite and the host rock are in the range 0.01–0.02; interestingly, when considering the observed seismic anisotropy of the mylonitic rocks, the coefficients are higher (0.02–0.03) with the highest value obtained in the most-deformed sample (KB4). It is worth noting that even these relatively small values can produce significant reflections, especially when low-angle laminated geometries are involved as occurs within shear zones (e.g. Fountain, Hurich & Smithson, 1984; Hurich & Smithson, 1987; Hurich, Deemer & Indares, 2001; Ross *et al.* 2004; Brown *et al.* 2012). As a consequence, within the shear zone the field mylonitic planar fabric (strike 199°; dip 14° ESE) could likely act as a reflector surface. It should however be noted that the thickness of the lithologic units is critical in any interpretation of reflectivity. A characteristic thickness of observable reflectors is estimated to be *c.* 20–200 m (e.g. Parsons, Howie & Thompson, 1992; Rey, Fountain & Clement, 1994) which is comparable with the estimated thickness of the shear zone (up to 200 m).

Results obtained clearly indicate the textural control (e.g. increasing CPO, especially of strongly anisotropic minerals, and grain size reduction) on the distribution of seismic anisotropy along a granitoid body within an extensional shear zone, therefore providing a link between microstructures, tectonics and the distribution of seismic properties. In addition, they allow large-scale seismic data, when available, to be better constrained and reflector geometries, together with the dynamics of crustal evolution, to be understood to a greater extent.

Acknowledgements. We thank Volker Feeser for the laboratory facilities and Detlef Schulte-Kortnak and Robert Hinkes for their technical support in Kiel. We are indebted to Salvatore Critelli for the critical reading of the manuscript. We are also grateful to Sebastiano Imposa for the constructive discussion about the seismic reflection coefficients and to Nino Lo Giudice for his valuable help. Finally, we thank Mark Allen, Telemaco Tesei and an anonymous reviewer for the suggestions that improved the paper. This work was supported by PRIN 2009 (research project grant by the Italian MIUR), project title 'Tectono-metamorphic evolution of the crystalline basement units of the eastern sector of the Rhodope Massif'.

References

ALMQVIST, B. S. G., HIRT, A. M., HERWEGH, M., EBERT, A., WALTER, J. M., LEISS, B. & BURLINI, L. 2013. Seismic anisotropy in the Morcles nappe shear zone: Implications for seismic imaging of crustal scale shear zones. *Tectonophysics* **603**, 162–78.

BAKER, J. H. & LIATI, A. 1991. The Oligocene volcano-sedimentary sequence of the Dipotama Basin, N. Greece: temporal relationships between Tertiary granites and volcanics, and implications for the regional tectonic evolution. *Geologie en Mijnbouw* **70**, 75–83.

BARRUOL, G., MAINPRICE, D., KERN, H., DE SAINT BLANQUAT, M. & COMPTE, P. 1993. 3D seismic study of a ductile shear zone from laboratory and petrofabric data (Saint Barthélémy Massif, Northern Pyrénées, France). *Terra Nova* **4**, 63–76.

BONCHEV, E. 1988. Notes on the alpine tectonics of the balkans. [Notes sur la tectonique alpine des Balkans] *Bulletin de la Société Géologique de France* **4**(2), 241–9.

BROWN, D., ZHANG, X., PALOMERAS, I., SIMANCAS, F., CARBONELL, R., JUHLIN, C. & SALISBURY, M. 2012. Petrophysical analysis of a mid-crustal reflector in the IBERSEIS profile, SW Spain. *Tectonophysics*, **550–3**, 35–46.

BRUN, J.-P. & SOKOUTIS, D. 2007. Kinematics of the Southern Rhodope Core Complex (North Greece). *International Journal of Earth Sciences* **96**(6), 1079–99.

BURG, J. 2012. Rhodope: From Mesozoic convergence to Cenozoic extension. Review of petro-structural data in the geochronological frame. In *The Geology of Greece* (eds E. Skourtsos & G. S. Lister). *Journal of the Virtual Explorer* **42**, paper 1; electronic edition ISSN 1441-8142.

BURG, J. P., RICOU, L. E., IVANOV, Z., GODFRIAUX, I., DIMOV, D. & KLAIN, L. 1996. Syn-metamorphic nappe complex

https://doi.org/10.1017/S001675681300109X Published online by Cambridge University Press

in the Rhodope massif: structure and kinematics. *Terra Nova* **8**(1), 6–15.

BURLINI, L. & KUNZE, K. 2000. Fabric and seismic properties of Carrara marble mylonites. *Physics and Chemistry of the Earth* **25**, 133–9.

CARACCIOLO, L., CRITELLI, S., INNOCENTI, F., KOLIOS, N. & MANETTI, P. 2011. Unraveling provenance from Eocene–Oligocene sandstones of the Thrace Basin, North-east Greece. *Sedimentology* **58**, 1988–2011.

CARACCIOLO, L., CRITELLI, S., INNOCENTI, F., KOLIOS, N. & MANETTI, P. 2013. Reply to the Discussion by Maravelis and Zelilidis on 'Unravelling provenance from Eocene–Oligocene sandstones of the Thrace Basin, North-east Greece' by Caracciolo *et al.* (2011), *Sedimentology* **58**, 1988–2011. *Sedimentology* **60**(3), 865–9.

CARACCIOLO, L., VON EYNATTEN, H., TOLOSANA-DELGADO, R., CRITELLI, S., MANETTI, P. & MARCHEV, P. 2012. Petrological, geochemical, and statistical analysis of Eocene-Oligocene sandstones of the Western Thrace Basin, Greece and Bulgaria. *Journal of Sedimentary Research* **82**, 482–98.

CIRRINCIONE, R., FAZIO, E., FIANNACCA, P., ORTOLANO, G. & PUNTURO, R. 2009. Microstructural investigation of naturally deformed leucogneiss from an Alpine shear zone (southern Calabria, Italy). *Pure and Applied Geophysics* **166**, 995–1010.

CIRRINCIONE, R., FAZIO, E., HEILBRONNER, R., KERN, H., MENGEL, K., ORTOLANO, G., PEZZINO, A. & PUNTURO, R. 2010. Microstructure and elastic anisotropy of naturally deformed leucogneiss from a shear zone in Montalto (southern Calabria, Italy). *Journal of The Geological Society* **332**, 49–68.

CIRRINCIONE, R., FAZIO, E., ORTOLANO, G., PEZZINO, A. & PUNTURO, R. 2012. Fault-related rocks: deciphering the structural-metamorphic evolution of an accretionary wedge in a collisional belt, NE Sicily. *International Geology Review* **54**(8), 940–56.

DAVIS, G. A. & CONEY, P. J. 1979. Geological development of metamorphic core complexes. *Geology* **7**, 120–4.

DEL MORO, A., KYRIAKOPOULOS, K., PEZZINO, A., ATZORI, P. & LO GIUDICE, A. 1990. The metamorphic complex associated to the Kavala plutonites: a Rb–Sr geochronological, structural and petrological study. *Geologica Rhodopica* **2**, 143–56.

DEWEY, J. F. 1988. Extensional collapse of orogens. *Tectonics* **7**, 1123–39.

DEWEY, J. F., PITMAN III, W. C., RYAN, W. B. F. & BONNIN, J. 1973. Plate tectonics and the evolution of the alpine system. *Bulletin of the Geological Society of America* **84**(10), 3137–80.

DIMADIS, E. & ZACHOS, S. 1989. Geological and tectonic structure of the metamorphic basement of the Greek Rhodope. *Geologica Rhodopica* **1**, 122–30.

DINTER, D. A., MACFARLANE, A., HAMES, W., ISACHSEN, C., BOWRING, S. & ROYDEN, L. 1995. U–Pb and 40Ar/39Ar geochronology of the Symvolon granodiorite: implications for the thermal and structural evolution of the Rhodope metamorphic core complex, northeastern Greece. *Tectonics* **14**, 886–908.

DINTER, D. A. & ROYDEN, L. 1993. Late Cenozoic extension in northeastern Greece: Strymon Valley detachment system and Rhodope metamorphic core complex. *Geology* **21**(1), 45–8.

DURR, S., ALTHERR, R., KELLER, J., OKRUSCH, M. & SEIDEL, E. 1978. The median Aegean crystalline belt: structure, metamorphism, magmatism. In *Alps, Appenines, Hellenides – Geodynamic Investigation Along Geotraverses by an International Group of Scientists* (eds H. Closs, D. Roeder & K. Schmidt), pp. 445–77. IUGS, Stuttgart, Scientific Report **38**.

ELEFTHERIADIS, G. & KORONEOS, A. 2003. Geochemistry and petrogenesis of post-collision pangeon granitoids in central macedonia, northern greece. *Chemie Der Erde: Geochemistry* **63**(4), 364–89.

FAZIO, E., PUNTURO, R. & CIRRINCIONE, R. 2010. Quartz c-axis texture mapping of mylonitic metapelite with rod structures (Calabria, southern Italy): clues for hidden shear flow direction. *Journal of the Geological Society of India* **75**(1), 171–82.

FOSTER, D. A., SCHAFER, C., FANNING, C. M. & HYNDMAN, D. W. 2001. Relationships between crustal partial melting, plutonism, orogeny, and exhumation: Idaho-bitterroot batholith. *Tectonophysics* **342**(3–4), 313–50.

FOUNTAIN, D. M., HURICH, C. A. & SMITHSON, S. B. 1984. Seismic reflectivity of mylonite zones in the crust. *Geology* **12**, 195–98.

FRANZINI, M., LEONI, L. & SAITTA, M. 1975. Revisione di una metodologia analitica per fluorescenza-X, basata sulla correzione completa degli effetti di matrice. *Rendiconti della Società Italiana di Mineralogia e Petrologia* **31**, 365–78.

GAPAIS, D. 1989. Shear structures within deformed granites: thermal and mechanical indicators. *Geology* **17**, 1144–7.

GUEYDAN, F., MEHL, C. & PARRA, T. 2005. Stress-strain rate history of a midcrustal shear zone and the onset of brittle deformation inferred from quartz recrystallized grain size. In *Deformation Mechanisms, Rheology and Tectonics: From Minerals to Lithosphere* (eds D. Gapais, J. P. Brun & P. R. Cobbold), pp. 127–42. Geological Society of London, Special Publication no. **243**.

HACKER, B. R. & ABERS, G. A. 2004. Subduction Factory 3. An Excel worksheet and macro for calculating the densities, seismic wave speeds, and H2O contents of minerals and rocks at pressure and temperature. *Geochemistry, Geophysics, Geosystems* **5**, Q01005, doi: 10.1029/2003GC000614.

HURICH, C. A., DEEMER, S. J. & INDARES, A. 2001. Compositional and metamorphic controls on velocity and reflectivity in the continental crust: an example from the Grenville Province of eastern Quebec. *Journal of Geophysical Research* **106**, 665–82.

HURICH, C. A. & SMITHSON, S. B. 1987. Compositional variation and the origin of deep crustal reflections. *Earth Planetary Science Letters* **85**(4), 416–26.

JACKSON, J. A. & WHITE, N. J. 1989. Normal faulting in the upper continental crust: observations from regions of active extension. *Journal of Structural Geology* **11**, 15–36.

JONES, C. E., TARNEY, J., BAKER, J. H. & GEROUKI, F. 1992. Tertiary granitoids of Rhodope, northern Greece: magmatism related to extensional collapse of the Hellenic orogen? *Tectonophysics* **210**, 295–314.

KERN, H. 1982. Elastic-wave velocity in crustal and mantle rocks at high pressure and temperature: the role of the high-low quartz transition and of dehydration reactions. *Physics of the Earth and Planetary Interiors* **29**(1), 12–23.

KERN, H., LIU, B. & POPP, T. 1997. Relationship between anisotropy of P and S wave velocities and anisotropy of attenuation in serpentinite and amphibolite. *Physics of the Earth and Planetary Interiors* **175**, 151–66.

KERN, H. & WENK, H.-R. 1990. Fabric-related velocity anisotropy and shear wave splitting in rocks from the Santa

Rosa Mylonite Zone, California. *Journal of Geophysical Research* **95**, 11 213–23.

KHAZANEHDARI, J., RUTTER, E. H., CASEY, M. & BURLINI, L. 1998. The role of crystallographic fabric in the generation of seismic anisotropy and reflectivity of high strain zones in calcite rocks. *Journal of Structural Geology* **20**, 293–9.

KILIAS, A., FALALAKIS, G. & MOUNTRAKIS, D. 1999. Cretaceous-tertiary structures and kinematics of the serbomacedonian metamorphic rocks and their relation to the exhumation of the Hellenic hinterland (Macedonia, Greece). *International Journal of Earth Sciences* **88**(3), 513–31.

KILIAS, A., FRISCH, W., AVGERINAS, A., DUNKL, I., FALALAKIS, G. & GAWLICK, H. 2010. Alpine architecture and kinematics of deformation of the northern pelagonian nappe pile in the Hellenides. *Austrian Journal of Earth Sciences* **103**(1), 4–28.

KILIAS, A. & MOUNTRAKIS, D. 1990. Kinematics of the crystalline sequences in the western Rhodope massif. *Geologica Rhodopica* **2**, 100–16.

KOLOCOTRONI, C. & DIXON, J. E. 1991. The origin and emplacement of the Vrondou granite, Serres, NE Greece. *Bulletin of the Geological Society of Greece* **25**(1), 469–83.

KYRIAKOPOULOS, K., PEZZINO, A. & DEL MORO, A. D. 1989. Rb–Sr geochronological, petrological and structural study of the Kavala plutonic complex (N. Greece). *Bulletin of the Geological Society of Greece* **23**, 545–60.

LE MAITRE, R. W. 1979. A new generalised petrological mixing model. *Contributions to Mineralogy and Petrology* **71**(2), 133–7.

LIATI, A. 1988. Corundum- and zoisite-bearing marbles in the rhodope zone, xanthi area (N. Greece): estimation of the fluid phase pomposition. *Mineralogy and Petrology* **38**(1), 53–60.

LIATI, A. & KREUZER, H. 1990. K–Ar dating of metamorphic and magmatic rocks from the Xanthi and Drama areas, Greek part of the Rhodope zone, Beih. z. *European Journal of Mineralogy* **2**(1), 161.

LIPS, A. L. W., WHITE, S. H. & WIJBRANS, J. R. 2000. Middle–Late Alpine thermotectonic evolution of the southern Rhodope Massif, Greece. *Geodinamica Acta* **13**, 281–92.

LISTER, G. S., BANGA, G. & FEENSTRA, A. 1984. Metamorphic core complexes of cordilleran type in the Cyclades, Aegean Sea, Greece. *Geology* **12**(4), 221–5.

MPOSKOS, E. & PERDIKATSIS, V. 1987. High-pressure metamorphism in East Rhodope Massif (Greece). *Fonschritte der Mineralogie* **65**(1), 140.

NEIVA, A. M. R., CHRISTOFIDES, G., ELEFTHERIADIS, G. & SOLDATOS, T. 1996. Geochemistry of granitic rocks and their minerals from the Kavala pluton, Northern Greece. *Chemie der Erde* **56**, 117–42.

PAPANIKOLAOU, D. & PANAGOPOULOS, A. 1981. On the structural style of southern Rhodope, Greece. *Geologica Balcanica* **11**, 13–22.

PARSONS, T., HOWIE, J. M. & THOMPSON, G. A. 1992. Seismic constraints on the nature of lower crustal reflectors beneath the extending southern transition zone of the Colorado Plateau, Arizona. *Journal of Geophysical Research* **97**, 12 391–407.

PASSCHIER, C. W., ZHANG, J. S. & KONOPASEK, J. 2005. Geometric aspects of synkinematic granite intrusion into a ductile shear zone-an example from the Yunmengshan core complex, northern China. *Journal of the Geological Society, London* **245**, 65–80.

PE-PIPER, G., PIPER, D. J. W. & MATARANGAS, D. 2002. Regional implications of geochemistry and style of emplacement of miocene I-type diorite and granite, Delos, Cyclades, Greece. *Lithos* **60**(1–2), 47–66.

PETRELLI, M., POLI, G., PERUGINI, D. & PECCERILLO, A. 2005. PetroGraph: A new software to visualize, model, and present geochemical data in igneous petrology. *Geochemistry, Geophysics, Geosystems* **6**(7), Q07011.

PUNTURO, R., CIRRINCIONE, R., FAZIO, E., FIANNACCA, P., KERN, H., MENGEL, K., ORTOLANO, G. & PEZZINO, A. 2012. Quartz deformation mechanisms in shear zones inferred by quantitative microstructural investigation: the case study of Kavala (Rhodope massif, north-eastern Greece). *Rendiconti Online Societa Geologica Italiana* **21**(1), 146–7.

REY, P. F., FOUNTAIN, D. M. & CLEMENT, W. P. 1994. P-wave velocity across a non-coaxial ductile shear zone and its associated strain gradient: consequences for upper crustal reflectivity. *Journal of Geophysical Research* **99**(B3), 4533–48.

ROSS, A. R., BROWN, L. D., PANANONT, P., NELSON, K. D., KLEMPERER, S., HAINES, S., WENJIN, Z. & JINGRU, G. 2004. Deep reflection surveying in central Tibet: lower crust layering and crustal flow. *Geophysical Journal International* **156**(1), 115–28.

SIIVOLA, J. & SCHMID, R. A. 2007. List of mineral abbreviations. In *Metamorphic Rocks: A Classification and Glossary of Terms* (eds D. Fettes and J. Desmons), pp. 93–110. Cambridge: Cambridge University Press.

SOKOUTIS, D., BRUN, J. P., VAN DEN DRIESSCHE, J. & PAVLIDES, S. 1993. A major Oligo-Miocene detachment in southern Rhodope controlling North Aegean extension. *Journal of the Geological Society, London* **150**, 243–6.

STRECKEISEN, A. & LE MAITRE, R. W. 1979. A chemical approximation to the modal QAPF classification of igneous rocks. *Neues Jahrbuch fur Mineralogie, Abhandlungen* **136**, 169–206.

TURNER, F. J. & WEISS, L. E. 1963. *Structural Analysis of Metamorphic Tectonites*. New York: McGraw-Hill, 545 pp.

TURPAUD, P. & REISCHMANN, T. 2010. Characterisation of igneous terranes by zircon dating: implications for UHP occurrences and suture identification in the Central Rhodope, northern Greece. *International Journal of Earth Sciences* **99**, 567–91.

VERNON, R. H. 1986. K-feldspar megacrysts in granites – phenocrysts, not porphyroblasts. *Earth-Science Reviews* **23**, 1–63.

WALCOTT, C. R. & WHITE, S. H. 1998. Constraints on the kinematics of post-orogenic extension imposed by stretching lineations in the aegean region. *Tectonophysics* **298**(1–3), 155–75.

WANG, Q., JI, S., SALISBURY, M. H., XIA, B., PAN, M. & XU, Z. 2005. Pressure dependence and anisotropy of P-wave velocities in ultrahigh- pressure metamorphic rocks from the Dabie–Sulu orogenic belt (China): implications for seismic properties of subducted slabs and origin of mantle reflections. *Tectonophysics* **398**, 67–99.

WERNICKE, B. 1985. Uniform-sense normal simple shear of the continental lithosphere. *Canadian Journal of Earth Sciences* **22**, 108–25.

ZACHOS, S. & DIMADIS, E. 1983. The geotectonic position of the Skaloti-Echinos granite and its relationship to

metamorphic formations of Greek Western and Central Rhodope. *Geologica Balcanica* **13**(5), 17–2.

ZAGORCHEV, I. S. 1998. Pre-priabonian Palaeogene formations in southwestern Bulgaria and northern Greece: stratigraphy and tectonic implications. *Geological Magazine* **135**(1), 101–19.

ZANANIRI, I., KONDOPOULOU, D., DIMITRIADIS, S. & KILIAS, A. 2013. Insights into the geotectonic evolution of the southern rhodope as inferred from a combined AMS, microtextural and paleomagnetic study of the tertiary symvolon and vrondou plutons. *Tectonophysics* **595–596**, 106–24.

https://doi.org/10.1017/S001675681300109X Published online by Cambridge University Press